PIEZOELECTRIC TRANSDUCTION MECHANISM FOR VIBRATION BASED ENERGY HARVESTING

A thesis submitted in the partial fulfilment

of the requirements for the degree of

Master of Technology

in

Mechanical Engineering

(Specialization: Machine Design and Analysis)

Submitted by

Himanshu Porwal

(Roll No: 211ME1161)

DEPARTMENT OF MECHANICAL ENGINEERING

NATIONAL INSTITUTE OF TECHNOLOGY

ROURKELA-769008, INDIA

JUNE 2013

PIEZOELECTRIC TRANSDUCTION MECHANISM FOR VIBRATION BASED ENERGY HARVESTING

A thesis submitted in the partial fulfilment

of the requirements for the degree of

Master of Technology

in

Mechanical Engineering

(Specialization: Machine Design and Analysis)

Submitted by

Himanshu Porwal

(Roll No: 211ME1161)

Under the esteemed guidance of

Prof. J. SRINIVAS

DEPARTMENT OF MECHANICAL ENGINEERING

NATIONAL INSTITUTE OF TECHNOLOGY

ROURKELA-769008, INDIA

JUNE 2013

DEPARTMENT OF MECHANICAL ENGINEERING
NATIONAL INSTITUTE OF TECHNOLOGY
ROURKELA, ODISHA-769008

CERTIFICATE

This is to certify that the thesis entitled "**PIEZOELECTRIC TRANSDUCTION MECHANISM FOR VIBRATION BASED ENERGY HARVESTING**" by '**Himanshu Porwal'**, submitted to the National Institute of Technology (NIT), Rourkela for the award of Master of Technology in **Machine Design and Analysis**, is a record of bona fide research work carried out by him in the Department of Mechanical Engineering, under our supervision and guidance.

I believe that this thesis fulfills part of the requirements for the award of degree of Master of Technology. The results embodied in the thesis have not been submitted for the award of any other degree elsewhere.

Place: Rourkela

Date:

Prof. J.Srinivas
Department of Mechanical Engineering
National Institute of Technology
Rourkela Odisha-769008

ACKNOWLEDGEMENT

First and foremost, I am truly indebted to my supervisor Prof. J. Srinivas for his inspiration, excellent guidance and unwavering confidence throughout my study, without which this thesis would not be in the present form.

I also thank him for his gracious encouragement throughout the work. I express my gratitude to Prof. S.C. Mohanty for his help in permitting to experimental work. I am also very much obliged to Prof. K.P. Maity, Head of the Department of Mechanical Engineering, NIT Rourkela for providing all possible facilities towards this work. I would also like to thank all my friends for extending their technical and personal support and making my stay pleasant and enjoyable.

Last but not the least, I mention my indebtedness to my father and mother for their love and affection and especially their confidence which made me believe me.

Himanshu Porwal

Rourkela, May 2013

ABSTRACT

Piezoelectric energy harvesting is a promising technology for extracting the power from environmental vibrations. It generates the electrical power of few orders of amplitudes which is sufficient to drive several autonomous electrical devices. Such vibration-based energy harvester generates the most energy when the generator is excited at its resonance frequency. When the external frequency shifts, the performance of the generator drastically reduces. In this line, present work first studies the various factors affecting the amount of power harvested. Simplest model to be started is with a single degree of freedom lumped parameter model of cantilever bimorph equivalent system with a tip-mass. To enhance the power harvesting capability of such simplest system over a wide bandwidth range, a two degree of freedom harvester system is explained in the present work. Its capability to work over a range of frequency is mathematically predicted. The system can be generalized for any number of degrees of freedom. The continuous beam models based on Euler and Rayleigh's theory are next import issues considered in this thesis. The equations of motion are obtained from Hamilton's principle and are solved by Galerkin's method with one mode approximation. Results are validated with lumped-parameter solutions. As a next step, the electroaeroelastic harvesting problem is considered to know the modeling issues and amount of power harvested. In aerofoil motion, plunge and pitch degrees of freedom are assumed and electrical field is coupled with plunge degree of motion. The resultant coupled elctromechanical equations are solved using fourth order Runge-Kutta time integration scheme. Results are satisfactory when compared with published data. Finally, an experimental analysis is conducted at laboratory level by providing the sinusoidal base excitation using a vibration shaker to a thin brass BZT bimorph cantilever with tip-mass. The open-circuit voltage history obtained from the piezoceramic layer is reported.

CONTENTS

LIST OF FIGURES

NOTATION

D_3 Electric displacement

σ_1 Axial stress of the piezoelectric material

S_1 Axial strain of the piezoelectric material

E_3 The electric field in each piezoelectric layer

v Voltage potential difference of each layer thickness

ε_{33}^{S} The permittivity of the piezoelectric material measured at constant stress

e_{31} The piezoelectric coupling coefficient

d_{31} Piezoelectric constant

c_{11}^{E} The elastic modulus for the piezoelectric material measured at constant electric field

E_s The elastic modulus for the substrate material

t_p The thickness of piezoceramic layer

t_s The thickness of substrate layer

l_p Length of Piezo layer

l_s Length of substrate layer

ρ_s Density of substrate

ρ_p Density of piezo layer

V_s Volume of substrate

V_p Volume of piezolayer

w Width of both Piezo and substrate layer

θ Electro-mechanical coupling co-efficient

m_t Tip mass

δT	Kinetic energy
δW	Work done
δU	Potential Energy
M_{rl}	Mass matrix
C	Structural damping matrix
K_{rl}	Stiffness matrix
y	Displacement of beam
v	Voltage across resistor
C_p	Piezoelectric capacitance
ϕ_{rl}	Mode shape function of the beam
β_r	Frequency factor
σ	Stress
S	Strain
b	Damping co-efficient
b_1	Damping co-efficient for mass 1
b_2	Damping co-efficient for mass 2
q	Electrical charge
f_i	Non-conservative force
R	Resistance
B	Displacement of beam
m_T	The total mass of the wing including its support structure
m_w	The wing mass alone
c_h and c_α	The plunge and pitch structural damping coefficients;

k_h and k_α The linear structural stiffnesses for the plunge and pitch degrees of freedom

k_{h2} and $k_{\alpha 2}$ The nonlinear stiffnesses of the plunge and pitch degrees of freedom

θ and χ Electromechanical coupling terms

I_α Mass moment of inertia about the elastic axis

L Aerodynamic lift about the elastic axis

M Aerodynamic moment about the elastic axis

x_α Eccentricity between centre of mass and elastic axis

U Free stream Velocity

ω Natural Frequency of beam

CHAPTER-1

INTRODUCTION

1.1 AMBIENT ENERGY HARVESTING

Energy harvesting from ambient vibrations by using various form of transduction has been recognized as a viable means for powering small electronic devices and remote sensors in order to eliminate their dependence on external power sources such as batteries or power grids. With such self-powered capabilities, these devices and sensors can operate in an uninterrupted fashion over prolonged periods of time. In recent years, interest in energy harvesting has increased rapidly, and harvesting vibration energy using piezoelectric materials has attracted a great deal of attention. Different types of piezoelectric transducer can be used to harvest vibration energy, including monomorph, bimorph, stack or membrane. Each configuration has its own advantages and limitations, and in general it is not possible for an energy harvester to perform well in all applications. For this reason, energy harvesters are normally designed for a specific application and a particular frequency range of operation.

There is another aspect of energy harvesting from the aerofoil wing sections and cylinders. The new studies have focused on harvesting energy from aeroelastic systems, in which energy is harvested from the airfoil section which is connected to a torsional bar which act as a cantilever beam because it is fixed at one end. For harvesting the energy, the piezo patches are laid down over the torsional bar. The power is harvested when the wind passes through the aerofoil and when the wind velocity crosses the critical speed which is called flutter speed. The amount of energy that can be extracted from such a aeroelastic system depends on its parameters and the wind speed.

Electromagnetic, electrostatic and piezoelectric transductions are the three basic conversion mechanisms commonly used to convert the basic vibrations to electrical energy. Energy density of piezoelectric mechanism is three times higher compared to other means. Piezoelectric cantilever beams are widely used structures in energy harvesting applications due to their high flexibility and low natural frequency. Often a tip-mass is attached to the free end of the cantilever to reduce its natural frequency and increase its deflection. A symmetrical piezoelectric layers when attached to the parent shim surface of the cantilever, it is known as a bimorph beam shown in Fig.1.1.

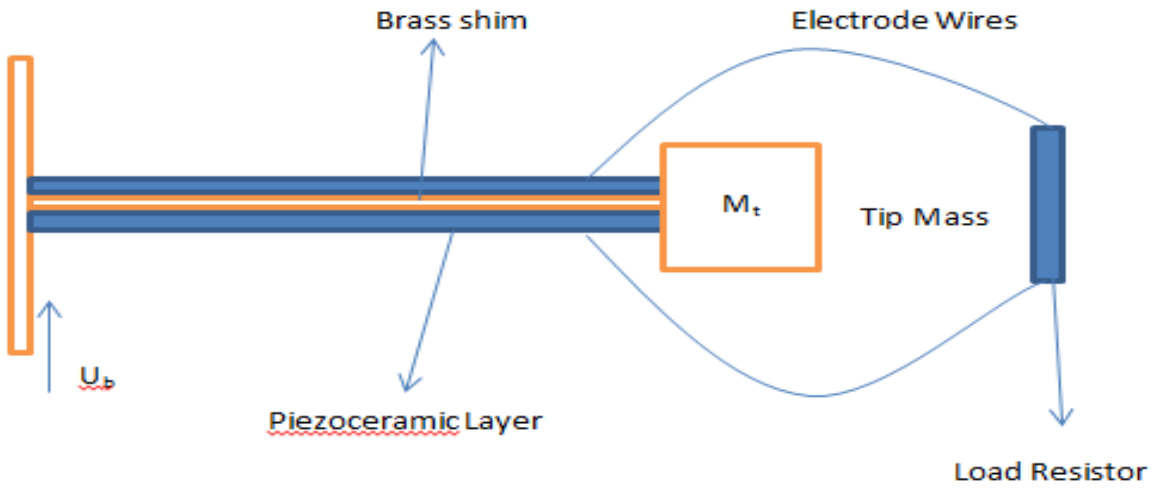

Fig.1.1 Energy harvesting from piezoelectric bimorph cantilever beam

When such a bimorph cantilever is put on a vibrating host structure, it generates an alternating voltage output for powering an electric load.

1.2 LITRATURE REVIEW

Piezoelectric materials, which directly convert mechanical strain to electrical energy, have been extensively investigated in recent years as a potential means to harvest energy from mechanical vibrations. This research has predominately focused on harvesting energy from preexisting

vibrating host structures through base excitation of cantilevered piezoelectric beams. Early in 2004, Mitcheson et al. [1] indicated that piezoelectric energy harvesters have a wider operating range than other energy harvesting transductors, especially when dealing with low-frequency ambient vibrations. Consequently, piezoelectric transduction has received the most attention. Many review papers have summarized the literature of piezoelectric energy harvesting [2–6]. The most common configuration for piezoelectric energy harvesting has been either a unimorph or a bimorph piezoelectric cantilever beam. Many studies on such configurations have been performed with the objective of maximizing the harvested electrical power [7-10].

1.2.1 Cantilever Beam Based structures

As shown in Fig.1.2, during power harvesting, a piezoelectric cantilever beam set into resonant motions via external excitations applied at its base.

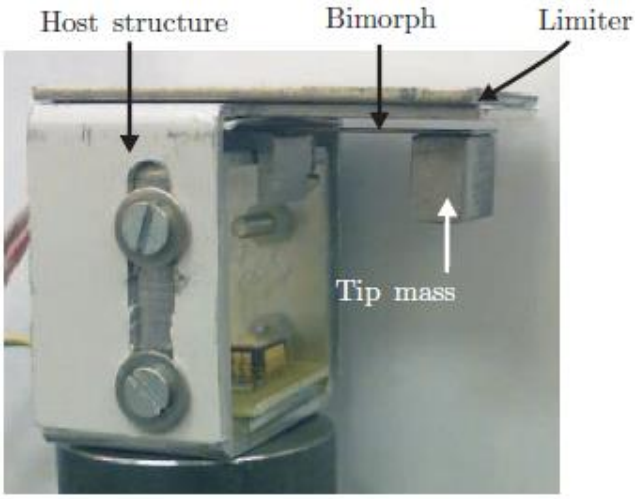

Fig.1.2 Generalized base excited bimorph cantilever with tip mass

Early works focused on the conversion of mechanical energy into electrical energy. In 1996, Umeda et al. [11] investigated the power generated when a free-falling steel ball impacted a plate with a piezoceramic wafer attached to its underside. Their study used an electrical equivalence

model to simulate the energy generated and calculate the ability of the PZT to transform mechanical impact energy into electrical power. It was found that a significant amount of the impact energy was returned to the ball in the form of kinetic energy during which the balls rebound off of the plate; however, it is stated that if the ball impacted the plate an efficiency of 52% could be achieved. In 1999, Goldfarb and Jones [12] presented a linearised model of a PZT stack and analysed its efficiency as a power generation device. It was shown that the maximum efficiency occurs in a low frequency region, much lower than the structural resonance of the stack. It is also stated that the efficiency is also related to the amplitude of the input force due to hysteresis of the PZT.

In 2001, Elvin et al. [13] theoretically and experimentally investigated a self-powered wireless sensors using PVDF. The power harvesting system used the energy generated by the PVDF to charge a capacitor and power a transmitter that could send information regarding the strain of the beam, a distance of 2 m.

In a basic work of electric power generation from piezoelectric materials, Sodano et al. [14] investigated the use of rechargeable batteries to accumulate the generated energy. The goal of this study was to show that the small amounts of ambient vibration found on a typical system could be used to charge the battery from its discharged state and demonstrated the compatibility of rechargeable batteries and the power generated by PZT materials. To do this, the vibration of the air compressor of a typical automobile was measured and a similar signal was applied to an aluminum plate with a PZT patch attached. It was found that the random signal from the engine compartment of a car could charge the battery in only a couple of hours and that a resonant signal could charge the battery in under an hour.

Wu et al.[15] proposed the use of a tunable resonant frequency power harvesting device to continuously match the time-varying frequency of the external vibration in real time.

Aldraihem and Baz [16] presented the concept of dynamic magnifier as applied to a single degree of freedom harvester. Wang et al. [17] presented a type of vibration energy harvester combining a piezoelectric cantilever and a single degree of freedom elastic system. The function of additional single degree of freedom system is to magnify vibration displacement of the piezoelectric cantilever to improve the power output.

Many finite element analysis studies were also shown in literature. Kim and Kim [18] described the development of an enhanced beam model with which the electrical outputs of a cantilevered piezoelectric energy harvester having a moderate aspect ratio and distributed tip mass could be accurately evaluated under harmonic base vibration. ANSYS software is employed in this line. Zhou et al. [19] proposed a model to predict the energy harvesting performance of shear mode piezoelectric cantilever by combining a single degree of freedom model with electrical model. The experimental results are validated with ANSYS solutions.

In another interesting article, Mak et al. [20] described their set-up with bump-stop in design of piezoelectric bimorph cantilever beam energy harvester to limit the maximum displacement of cantilever and prevent excessive high bending stresses to be developed as a result of shock. Results of theoretical model were validated with an experiment. In a recent article, Erturk [21], presented a generalized framework for electromechanical modeling of base-excited piezoelectric energy harvesters with symmetric and unsymmetric laminates. The derivations are given using the assumed-modes method under the Euler-Bernoull, Rayleigh and Timoshenko beam assumptions. More recently, Zhao and Erturk [22] presented electroelastic

modeling of piezoelectric energy harvesting from broadband random vibrations, based on distributed parameter model by considering tip-mass.

Tang and Yang [23] presented a generalized multiple-degree of freedom piezoelectric energy harvesting model to adapt in frequency-variant scenarios. It overcomes the bandwidth issues and gets effective power harvesting ability. Experimental work and numerical analysis using ANSYS were presented in this work. Lumentut and Howard [24] presented an analytical method for modeling electromechanical piezoelectric bimorph beam with tip-mass under two input base transverse and longitudinal excitations using Euler's beam theory. In the same line, Wang and Meng [25] also presented the model of the dynamic behavior of an electromechanical piezoelectric bimorph cantilever harvester connected with an AC-DC circuit based on the Euler's theory. In another recent article, Cassidy and Scruggs [26] addressed the formulation of nonlinear feedback controllers for stochastically excited vibratory piezoelectric energy harvesters.

1.2.2 Piezo aeroelastic Energy harvesters

During the last decade, many new concepts for energy harvesting have been introduced and exploited to harness wasted energy from the environment. Another form of energy available in the vicinity of sensor nodes and remotely operating engineering systems is due to airflow. As an alternative to miniaturized windmill configurations, researchers have recently considered exploiting aeroelastic vibrations for converting wind energy into electricity using scalable configurations. An early experimental effort of generating electricity from thin curved airfoils with macrofiber composite piezoelectric structures under airflow excitation.

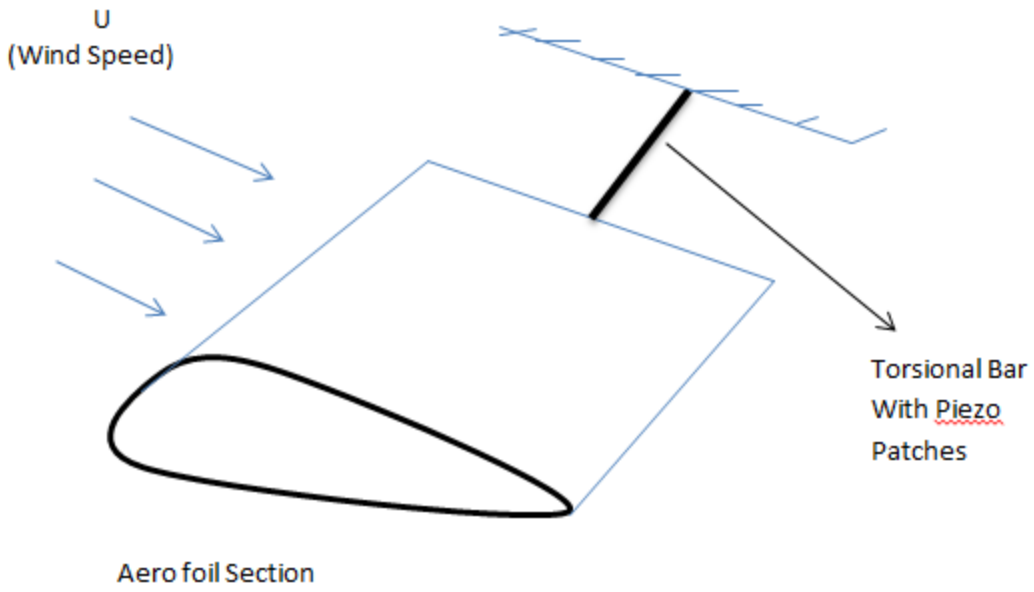

Fig 1.3 Piezoaeroelastic Model

Bryant et al. [27] demonstrated experimentally that energy can be harvested from aeroelastic vibrations using an airfoil section attached to a cantilever. Erturk et al. [28] used a lumped parameter wing-section model to determine the effects of piezoelectric power generation on the linear flutter speed. An electrical power output of 10.7 mW is delivered to a 100 kΩ load at the linear flutter speed of 9.30 m/s (which is 5.1% larger than the short-circuit flutter speed). The effect of piezoelectric power generation on the linear flutter speed is also discussed and a useful consequence of having nonlinearities in the system is addressed.

De Marqui et al. [29] used a finite element method to analyze piezoaeroelastic energy harvesters. In this work, an electromechanically finite element model is combined with an unsteady aerodynamic model to develop a piezoaeroelastic model for airflow excitation of cantilevered plates representing wing like structures. The electrical power output and the displacement of wing tip are investigated for several airflow speeds. More recently, researchers have focused on nonlinear aspects of aeroelastic energy harvesting using piezoelectric

transduction and airfoil configurations. Abdelkefi et al. [30-31] considered nonlinear plunge and pitch stiffness components, by nonlinear torsional and flexural springs in the pitch and plunge motions, respectively, with a piezoelectric coupling attached to the plunge degree of freedom. The analysis showed that the effect of the electrical load resistance on the flutter speed is negligible in comparison to the effects of the linear spring coefficients. De Marqui and Erturk [32] analyzed the airfoil based aeroelastic energy harvesting with piezoelectric transduction and electromagnetic induction separately. By considering two degree of freedom model by adding piezoelectric effect, the influence of several parameters in linear flutter speed zone were estimated.

1.3 SCOPE AND OBJECTIVES

Based on the above literature, there seems to be a wide scope in working with modeling issues as well with experimental findings. Standard beam formulations including continuous beam theory, single and multi-degree of freedom lumped-parameter modeling as well numerical analysis of such anisotropic structures is of fundamental interest in modern machine design and analysis arena. In this line, it is planned to develop accurate models of the mesoscale beam geometry for power harvesting application. Following are the objectives of the present work:

(i) Formulate the lumped-parameter model for a piezoelectric bimorph cantilever and study the amount of power harvested under various conditions.

(ii) Formulate and solve the continuous system model of the bimorph cantilever and validate the results of analysis with lumped-parameter models

(iii) Use finite element analysis tool to simulate the dynamics of piezoelectric bimorph cantilever beam to know the response behavior.

(iv) Conduct an experimental analysis to know the amount of output voltage harvested using the laboratory excitation sources.

(v) To under various other possible ways to harvest the energy using piezoelectric transduction mechanism.

1.4 Thesis Organization

The thesis is organized as follows:

Chapter-1 includes the introduction of ambient energy harvesters and aerofoil wing section energy harvester. This chapter also includes the literature review which is followed by future and scope of the energy harvesters.

Chapter-2 presents the mathematical modeling issues relating to various models employed in present work.

Chapter-3 deals with the details of experimental analysis conducted in the present work.

Chapter-4 presents finite element analysis of Piezoelectric cantilevered bimorph model.

Chapter-5 Presents the Results and discussions of the above described model.

Chapter-6 presents the conclusions of the above described contents.

CHAPTER-2

MATHEMATICAL MODELLING

This chapter explains various mathematical models used during analytical simulations for piezoelectric energy harvesting.

2.1 DISTRIBUTED PARAMETER MODEL

Distributed parameter modeling of bimorph cantilever beams gives an accurate representation of a real time system. Here, the systems are described by a set of coupled partial differential equations obtained from well-known Lagrange's principle or by principle of virtual work. There are several methods to solve these differential equations. The bimorph-piezoelectric cantilever beam energy harvester considered is shown in Fig. 2.1, in which two identical piezoelectric layers are attached to the substrate beam.

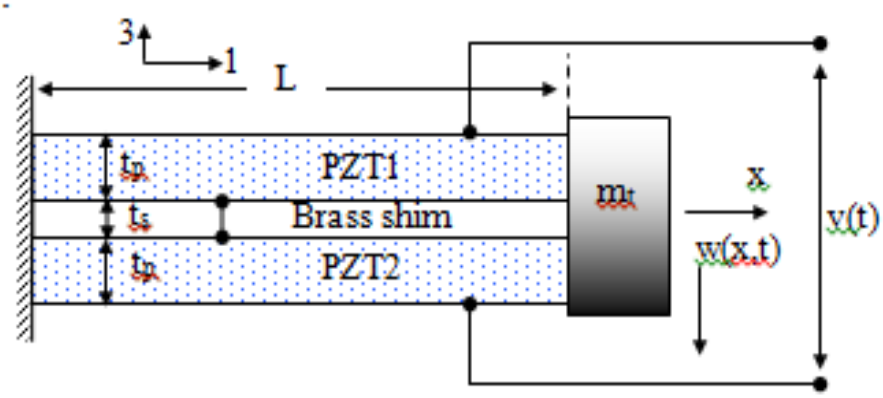

Fig 2.1Piezoelectric Cantilever Model

The piezoelectric layers can be connected in series or in parallel. For series connection, the positive polarity of PZT's are considered at uppermost layers and negative polarity at innermost

layers. For parallel connection, there is a alternation manner of polarity i.e. positive, negative, positive, negative.

The tip has a mass m_t. The piezoelectric material generates electrical charge through the thickness (3-direction) of the piezoelectric layer as the beam vibrates in the direction-3 with strain in the direction-1. The piezoelectric effect that couples the mechanical and electrical properties is described using the following linear constitutive equations for piezoelectric materials,

$$\begin{bmatrix} \sigma_1 \\ D_3 \end{bmatrix} = \begin{bmatrix} c_{11}^E & -e_{31} \\ e_{31} & \varepsilon_{33}^S \end{bmatrix} \begin{bmatrix} S_1 \\ E_3 \end{bmatrix} \tag{2.1}$$

In these equations, D_3 is the electric displacement, while $\sigma_1$and $S_1$are the axial stress and strain of the piezoelectric material, respectively. The electric field in each piezoelectric layer E_3 is assumed to be uniform throughout the entire layer and is defined as ratio of voltage potential difference of each layer v(t)/2 and the thickness t_p: $E_3=v(t)/2t_p$. The elastic modulus for the piezoelectric material c_{11}^E is measured at constant electric field, while the permittivity of the piezoelectric material ε_{33}^S is measured at constant stress. The piezoelectric coupling coefficient $e_{31}$is a product of the piezoelectric constant d_{31} and the elastic modulus: $e_{31}=d_{31}c_{11}^E$.

The deformations are assumed to be small and the material behavior is assumed to be linear so that the material, geometric, and dissipative nonlinearities are not pronounced. The substructure layer is isotropic and the piezoceramic layer is transversely isotropic as it is poled in the thickness direction. The Euler–Bernoulli approach is used to modeled the energy harvester beam.

The derivation of equations of motion is explained from Hamilton's theorem as follows,

Variational Indicator (VI)= $\int_{t1}^{t2}[\delta T - \delta U + \delta W].dt = 0$ (2.2)

Where δT, δW , δU are first variations of kinetic energy, work done and total potential energy respectively. Here total kinetic energy is given by

$$T = \frac{1}{2}\int_{Vs} \rho_s \dot{y}^T \dot{y}.dV_s + \int_{Vp} \rho_p \dot{y}^T \dot{y}.dV_p \tag{2.3}$$

Likewise, potential energy

$$U = \frac{1}{2}\int_{Vs} S^T \sigma.dV_S + \frac{1}{2}\int_{VP} S^T \sigma.dV_P - \int_{Vp} E^T D.dV_p \tag{2.4}$$

Where S is strain vector, σ is the stress vector and the subscript s and p stands for substructure and piezoceramic respectively. E is the electrical field vector and D is the electrical displacement vector. The last term in the equation represents internal electrical energy.

Virtual work done by non-conservative forces and electrical charge,

$$\delta W = \sum_{i=1}^{nf} \delta y(x_i).f_i(x_i) - \sum_{j=1}^{nq} \delta V.q_j \tag{2.5}$$

Where δV is the virtual voltage and q_j is the electrical charge output flowing to the external resistor. Also δy is virtual displacement due to non-conservative forces f_i.

First variations are now substituted into Hamilton's principle and the electomechanical lagranges equations are written in the form of

$$\frac{d}{dt}\left(\frac{\partial T}{\partial Z_k}\right) - \left(\frac{\partial T}{\partial Z_k}\right) + \left(\frac{\partial U}{\partial Z_k}\right) = f_k \tag{2.6}$$

With the Euler-Bernoullii's beam model having transverse displacement at neutral axis considered as $y(x,t)=\sum_{r=1}^{N}\phi_r(x)w_r(t)$,(where $\phi_r(x)$ is r^{th} mode shape and N is number of modes), the equation of motion reduces from assumed modes method as:

$$M\ddot{w} + c\dot{w} + Kw - \theta v = f \tag{2.7}$$

$$C_p\dot{v} + \frac{v}{R} + \theta\dot{w}=0 \tag{2.8}$$

where w is the unknown generalized co-ordinate vector and the expressions for M, c, K and θ are given as follows:

$$M_{rl} = \left(\rho_s A + 2\rho_p A\right)\int_0^l \emptyset_r(x)\,\emptyset_l(x)dx \tag{2.9}$$

Stiffness, $K_{rl}=(E_sI_S + 2c_{11}^E I_{p)}\int_0^l \emptyset_r''(x)\,\emptyset_l''(x)dx$ (2.10)

The Damping coefficient accounting mechanical dissipation effects is assumed to be linearly proportional to mass and stiffness so that,

$$c=\alpha M_T+\beta K$$

Electromechanical Coupling Co-efficient,

$\theta_r=\int_0^{\ell} J_p\phi_r''(x)dx$, where $J_p=\frac{e_{31}}{t_p}\int_0^w\int_{z=\frac{t_s}{2}}^{\frac{t_s}{2}+t_p} z\,dy\,dz$ (2.11)

Here $e_{31}=E_pd_{31}$ is effective piezoelectric stress constant

Equivalent capacitance, $$C_p = \frac{l_b w_p \varepsilon_{33}^s}{2t_p} \tag{2.12}$$

Where l_p , w_p and t_p are the length , width and thickness of each piezoceramic layer respectively.

Effective force vector, $f= m_{br}\ddot{b}(t)$ (2.13)

Where b is a base displacement in transverse direction and m_{br} is given as follows

$m_{br} = -(\rho_s A_s + 2\rho_p A_p)\int_0^{\ell} \phi_r(x)dx$ (2.14)

In order to solve the equations, the mode functions $\phi_r(x)$ to be obtained correctly. As we know for the beam $\phi_r(x) = A_r cos\beta_r x + B_r sin\beta_r x + C_r cosh\beta_r x + D_r sinh\beta_r x$. (2.15)

Here βr is the frequency factor Frequency Factor,

$\beta^4 = \frac{\rho A\omega^2}{EI}$, ω=Natural frequency , ρA= $(\rho_s A_s + 2\rho_p A_p)$ and

EI=$(E_s I_S + 2c_{11}^E I_{p)}$ The constants A_r,B_r,C_r and D_r are obtained from the following boundary conditions,

1. At x=0, $\phi_r(x)=0$

2. At x=0, $\phi'_r(x)=0$ (slope)

3. At x=l, $EI\phi''_r(x)=0$ (Moment)

4. At x=l, $EI\,\phi_r''' = M_t\ddot{w}$ (Shear Force)

By substituting the boundary conditions and eliminating the constants, we get the following frequency equation:

$$\begin{vmatrix} (\sinh(\beta l)-\sin(\beta l)) + \alpha_0(\beta l)(\cosh(\beta l)-\cos(\beta l)) & (\cos(\beta l)+\cosh(\beta l)) - \alpha_0(\beta l)(\sin(\beta l)-\sinh(\beta l)) \\ \cos(\beta l)+\cosh(\beta l) & \sin(\beta l)+\sinh(\beta l) \end{vmatrix} = 0$$

(2.16)

It can be simplified as:

$1 + \cos(\beta l)\cosh(\beta l) + \alpha_0(\beta l)[\cos(\beta l)sinh(\beta l) - sin(\beta l)sinh(\beta l)] = 0$ (2.17)

α_0= Tip mass ratio= $\alpha_0 = \frac{M_t}{\rho Al}$

This equation gives the numerical values of β, indicating first, second and so on frequency factors as in simple cantilever beams.

After finding β and using the simplification as illustrated in Appendix, the final modeshape function

$$\phi_r(x) = \phi_n[(\cos(\beta_r x) - \cosh(\beta_r x)) + C_1(\sin(\beta_r x) - \sinh(\beta_r x))] \quad (2.18)$$

where

$$C_1 = \frac{(\sinh(\beta_r l) - \sin(\beta_r l)) + \alpha_0(\beta_r l)(\cosh(\beta_r l) - \cos(\beta_r l))}{(\cos(\beta_r l) + \cosh(\beta_r l)) - \alpha_0(\beta_r l)(\sin(\beta_r l) - \sinh(\beta_r l))}$$

Here, ϕ_n is normalization factor.

In the present work, only the first mode is accounted in order to compute stiffness, mass and electromechanical coupling terms. MATLAB software is used to program the various stages in obtaining the output voltage response history. Symbolic logic toolbox helps in getting the integrations and other evaluations and finally the numerical substitutions are made. The two coupled dynamic equations are solved using Runge-Kutta time-integration scheme after converting them into state space form. The solver evaluates the shortcircuit voltage and power developed according to the equation

$$Power(P) = \frac{V^2}{R} \quad (2.19)$$

2.2 LUMPED PARAMETER ANALYSIS

(a) SINGLE DEGREE OF FREEDOM MODEL-

A piezoelectric energy harvester is conventionally designed as a 1-DOF lumped parameter model to simplify the formulation procedure. This model is widely adopted in literature. Since this model provides the fundamental insights into the electromechanical coupled characteristics of the harvester, it is first reviewed. Schematic of the harvester model under base excitation is shown in Fig.2.2. The system has equivalent mass m, damping co-efficient b and stiffness k subjected to small base excitation. Here, R is parallel to load resistance, $\frac{1}{c_p}$ is capacitive nature of piezoelectric model in which equivalent capacitance is $c_p=\frac{\varepsilon_{33}^{S} w_p L_p}{2t_p}$ with t_p as thickness of piezoelectric layer and θ is a transfer factor between mechanical and electrical domains known as electromechanical coupling coefficient of the system, v(t) is voltage across R.

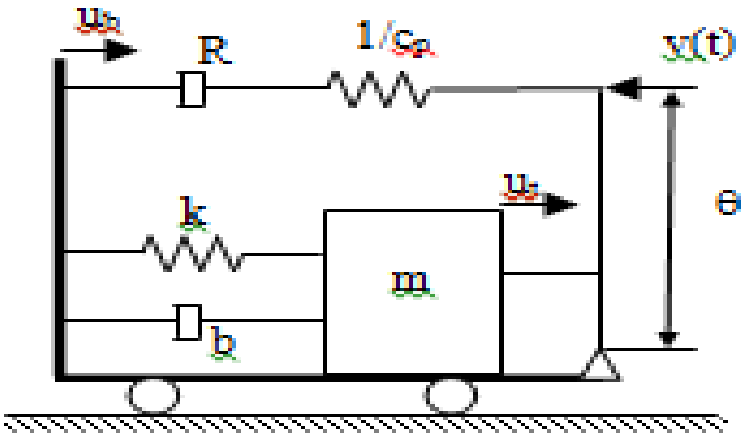

Figure2.2. Single Degree of Freedom Model

Writing equation of motion in terms of relative displacement: $u=u_t - u_b$, we obtain:

$$m\ddot{u} + b\dot{u} + ku = -m\ddot{u}_b - \theta v(t) \qquad (2.20)$$

Dividing by m both the sides, we can write:

$$\ddot{u} + 2\xi\omega_n\dot{u} + \omega_n^2 u = -\ddot{u}_b - \frac{\theta}{m}v \tag{2.21}$$

Where

$$\omega_n = \sqrt{\frac{k}{m}} \text{and} \frac{b}{m} = 2\xi\omega_n \tag{2.22}$$

The equivalent mass for a uniform cantilever beam loaded at its free end with tip mass m_t is given by: $m=m_t + \frac{33}{140}m_b$, with $m_b = \rho AL$ is the mass of the beam. The equivalent stiffness k can be written as: $k=\frac{3EI}{L^3}$. Here, the effective unit mass and flexural rigidity of the beam in terms of width b (assuming $w_p=w_s=w$) and thickness are given by [25]:

$$(\rho A)=w\,(\rho_S\, t_S + 2\rho_P\, t_P) \tag{2.23}$$

$$EI=E_s w\frac{t_s^3}{12} + 2c_{11}^E w\left(\frac{t_p^3}{12} + t_p\left(\frac{t_p+t_s}{2}\right)^2\right) \tag{2.24}$$

Equation relating the electrical parameters obtained from Kirchhoff's Law as:

$$-\theta\dot{u} + c_p\dot{v}(t) + \frac{v(t)}{R} = 0 \tag{2.25}$$

The above equations are coupled by the parameter θ. Assuming harmonic base motion and taking Laplace transforms,we get

$$ms^2\hat{u} + bs\hat{u} + k\hat{u} + \theta\hat{v} = -s^2 m\hat{u}_b \tag{2.26}$$

$$-\theta s\hat{u} + c_p s\hat{v} + \frac{\hat{v}}{R} = 0 \tag{2.27}$$

where s is Laplace variable, and the cap denotes a variable of function in the Laplace domain. Solving these algebraic equations and setting s=jΩ, we get the displacement and voltage magnitudes as:

$$U(\Omega) = \frac{m\Omega^2 U_b\left(\frac{1}{R}+jc_p\Omega\right)}{\left((k-m\Omega^2)+jb\Omega\right)\left(\frac{1}{R}+jc_p\Omega\right)+j\Omega\theta^2} \tag{2.28}$$

$$V(\Omega) = \frac{jU_b\theta\Omega^3}{\left((k-m\Omega^2)+jb\Omega\right)\left(\frac{1}{R}+jc_p\Omega\right)+j\Omega\theta^2} \tag{2.30}$$

In order to get power amplitude zone, one has to maximize the resonance bandwidth of a single degree of freedom oscillator.

(b) TWO DEGREE OF FREEDOM MODEL

By exploiting two degrees of freedom on adding a secondary spring-mass system as shown in Fig.2.3, the two peaks in wide frequency bandwidth may be observed. The parasitic subsystem composed of the mass m_2, spring stiffness k_2 and damping coefficient b_2. The equations of motion of the system can be written first in terms of parameters u_1, u_2 and u_b and then by setting $y=u_1-u_2$ and $u= u_1-u_b$, the governing equations of the model can be written as:

$$m_2\ddot{y} + b_2\dot{y} + k_2 y = -m_2\ddot{u} - m_2\ddot{u_b} \tag{2.31}$$

$$m\ddot{u} + b\dot{u} + ku - b_2\dot{y} - k_2 y + \theta v + m\ddot{u_b} = 0 \tag{2.32}$$

$$-\theta\dot{u} + c_p\dot{v}(t) + \frac{v(t)}{R} = 0 \tag{2.33}$$

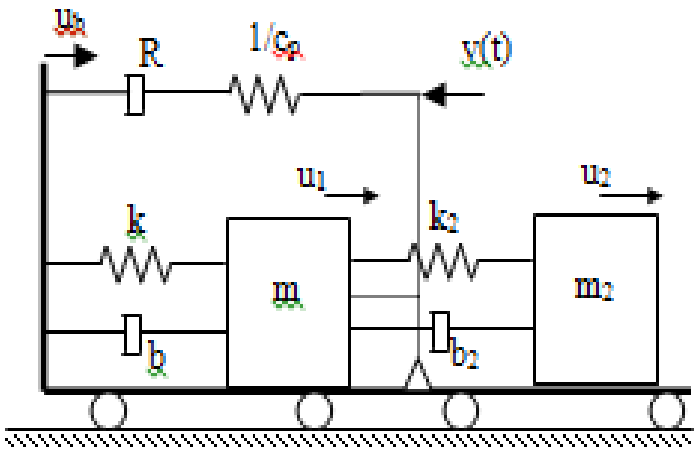

FIGURE 2.3 Two Degree of Freedom Model

Applying Laplace transform for these equations, we obtain:

$$m_2 s^2 \hat{u} + (m_2 s^2 + b_2 s + k_2)\hat{y} + m_2 s^2 \hat{u}_b = 0 \tag{2.34}$$

$$(ms^2 + bs + k)\hat{u} - (b_2 s + k_2)\hat{y} + \theta \hat{v} + ms^2 \hat{u}_b = 0 \tag{2.35}$$

$$-\theta s \hat{u} + \left(c^s s + \frac{1}{R_l}\right)\hat{v} = 0 \tag{2.36}$$

After solving these equations,

$$\hat{u} = -\frac{-(b_2 s + k_2)m_2 s^2 + ms^2(m_2 s^2 + b_2 s + k_2)}{\{(m_2 s^2 + b_2 s + k_2)(ms^2 + bs + k) + (b_2 s + k_2)m_2 s^2\}\left\{c_p s + \frac{1}{R}\right\} + \theta^2 s(m_2 s^2 + b_2 s + k_2)} \tag{2.37}$$

$$\hat{v} = \frac{\theta s}{\left(c_p s + \frac{1}{R}\right)}\hat{u} \tag{2.38}$$

Substituting s=jΩ and simplifying, we can obtain the frequency responses for displacement u and voltage v just like earlier case. Here, we define the non-dimensional parameters: $\mu = m_2/m_1$ and $\alpha = \omega_2/\omega_1$, where $\omega_1 = \sqrt{\frac{k_1}{m_1}}$ and $\omega_2 = \sqrt{\frac{k_2}{m_2}}$ to select the values of secondary system parameters m_2 and k_2.

Again MATLAB program is used to solve the dynamic equations of motion using time-integration scheme.

2.3 ENERGY HARVESTING THROUGH PIEZOAEROELASTIC VIBRATIONS

Previous studies have, in general, focused on harvesting energy from base vibrations. It is the new technique of harvesting energy from the aerorfoils. In present work, a piezoaeroelastic energy harvester consisting of a rigid aerorfoil constrained to pitch and plunge motions is considered and supported by torsional and flexural springs with a piezoelectric coupling attached to the plunge degree of freedom as shown in Fig.2.4.

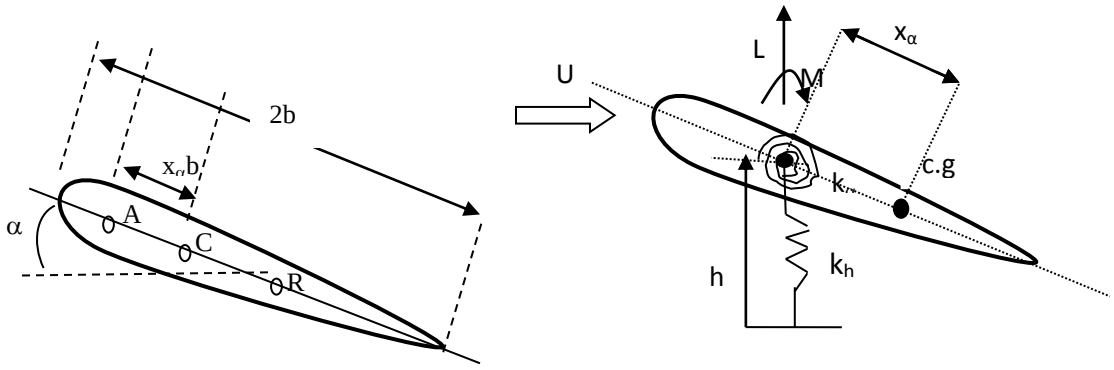

(a) Aerofoil cross-section (b) An aeroelastic system model with 2 degree of freedom The plunge displacement and pitch angle

Fig.2.4 Schematic of a piezoaeroelastic system under uniform airflow

Fig2.4(a) shows the cross-sectional view of an aero foil with all the centers i.e. A is an aerodynamic center(elastic axis), C is a geometric mass center and R is a reference point. 2b is a chord length of the aero foil. Fig2.4 (b) shows a two degree freedom of model i.e. plunge direction (h) and pitch angle (α). It also shows the lift force(L) opposite to the direction of deflection of aero foil with a moment(M) of aero foil.

When wind passes through this aerofoil section, aerodynamic lift forces are generated opposite to the deflection of aerofoil which creates an oscillation in the aerofoil which **i**s

transmitted to the torsional bar very nicely. This oscillation is sensed by the piezo-patches which then converted into electrical power by the help of electrical circuit attached to it .For the purpose of energy harvesting, it is important to generate energy at low wind speeds and, as such, to decrease the flutter speed. To harvest more energy, it would be better to minimize the energy distribution to the pitch motion when harvesting power from the plunge motion. The wing at a free stream velocity exhibits oscillations along a plunge displacement direction, and a rotation at the pitch angle around the elastic axis. The equations of motion of this system are written as :

$$m_T \ddot{h} + m_w x_\alpha b \ddot{\alpha} + c_h \dot{h} + (k_h + k_{h2} h^2) h - \theta V = -L \tag{2.39}$$

$$m_w x_\alpha b \ddot{h} + I_\alpha \ddot{\alpha} + c_\alpha \dot{\alpha} + (k_\alpha + k_{\alpha 2} \alpha^2) \alpha = M \tag{2.40}$$

$$c_p \dot{V} + \frac{V}{R} + \chi \dot{h} = 0 \tag{2.41}$$

Where,

m_T = The total mass of the wing including its support structure

m_w = The wing mass alone

c_h and c_α = The plunge and pitch structural damping coefficients;

k_h and k_α = The linear structural stiffnesses for the plunge and pitch degrees of freedom

k_{h2} and $k_{\alpha 2}$ = The nonlinear stiffnesses of the plunge and pitch degrees of freedom

θ and χ = Electromechanical coupling terms

I_α = Mass moment of inertia about the elastic axis

b = The half chord length

v = Voltage

L and M = aerodynamic lift and moment about the elastic axis

R = Load resistance

c_p =Capacitance of piezoelectric layer

x_α = Eccentricity between centre of mass and elastic axis

U = Free stream Velocity

Aerodynamic lift L=$\rho A U^2 b c_{l\alpha} \alpha_{effective}$ (2.42)

Aerodynamic Moment M= $\rho U^2 b^2 c_{m\alpha} \alpha_{effective}$ (2.43)

Where,

$$\alpha_{effective} = \alpha + \frac{\dot{h}}{U} + \left(\frac{1}{2} - a\right) b \frac{\dot{\alpha}}{U} \tag{2.44}$$

The matrix form of equation considering equation 1 and 2,

$$\begin{bmatrix} m_t & m_w b x_\alpha \\ m_w b x_\alpha & I_\alpha \end{bmatrix} \begin{bmatrix} \ddot{h} \\ \ddot{\alpha} \end{bmatrix} + \begin{bmatrix} k_h & \rho U^2 b c_l l \\ 0 & (k_\alpha - \rho U^2 b^2 c_m) \end{bmatrix} \begin{bmatrix} \dot{h} \\ \dot{\alpha} \end{bmatrix} + \begin{bmatrix} (c_h + \rho U b c_l l) & \rho U b^2 c_l l (\frac{1}{2} - a) \\ -\rho U b^2 c_m & (c_\alpha - \rho U b^3 c_m (\frac{1}{2} - a) \end{bmatrix} \begin{bmatrix} h \\ \alpha \end{bmatrix}$$

$$= 0 \tag{2.45}$$

The above equation is the form of following generalized equation of motion,

$$M\ddot{x} + C\dot{x} + Kx = 0 \tag{2.46}$$

Compare the equation2.45 with the above generalized equation. The state space form solution of the above equation is as follows,

$$\begin{bmatrix} \dot{x}_1 \\ \dot{x}_2 \end{bmatrix} = \begin{bmatrix} o_{2x2} & I_{2x2} \\ -M^{-1}K & -M^{-1}C \end{bmatrix} \begin{bmatrix} x_1 \\ x_2 \end{bmatrix} + \begin{bmatrix} 0 \\ M^{-1}F \end{bmatrix} \tag{2.47}$$

Where,

Mass matrix, Stiffness Matrix,

$$[M]=\begin{bmatrix} m_t & m_w b x_\alpha \\ m_w b x_\alpha & I_\alpha \end{bmatrix} \qquad [K]=\begin{bmatrix} k_h & \rho U^2 b c_l l \\ 0 & (k_\alpha - \rho U^2 b^2 c_m) \end{bmatrix}$$

Damping matrix,

$$[C]=\begin{bmatrix} (c_h + \rho U b c_l l) & \rho U b^2 c_l l(\frac{1}{2}-a) \\ -\rho U b^2 c_m & (c_\alpha - \rho U b^3 c_m(\frac{1}{2}-a) \end{bmatrix} \tag{2.48}$$

$$\left[M^{-1}K\right]=\left(\frac{1}{d}\right)\begin{bmatrix} I_\alpha K_h & I_\alpha(\rho U^2 b c_l l) - m_w b x_\alpha (k_\alpha - \rho U^2 b^2 c_m) \\ -m_w b x_\alpha K_h & -m_w b x_\alpha(\rho U^2 b c_l l) + m_t(K_\alpha - (\rho U^2 b^2 c_m) \end{bmatrix} \tag{2.49}$$

$$\left[M^{-1}C\right]=\frac{1}{d}\begin{bmatrix} I_\alpha(c_h + \rho U b c_l l) + (m_w b x_\alpha)\rho U b_2 c_m & I_\alpha \rho U b^2 c_l l(\frac{1}{2}-a) - (m_w b x_\alpha)(c_\alpha - \rho U b^3 c_m)(\frac{1}{2}-a) \\ (m_w b x_\alpha)(c_h + \rho U b c_l l) - m_t \rho U b^2 c_m & (m_w b x_\alpha)\rho U b^2 c_l l(\frac{1}{2}-a) + m_t(c_\alpha - \rho U b^3 c_m(\frac{1}{2}-a)) \end{bmatrix} \tag{2.50}$$

$$d = I_\alpha m_t - (m_w b x_\alpha)^2$$

The state space form of equation is as follows,

$$\dot{X} = [A]X + [B]U$$

Now the combined state space form of equation including equation.3 is as follows,

$$\begin{bmatrix} \dot{h} \\ \dot{\alpha} \\ \ddot{h} \\ \ddot{\alpha} \\ \dot{v} \end{bmatrix} = \begin{bmatrix} O_{2X2} & I_{2x2} & 0 \\ & & 0 \\ M^{-1}K & M^{-1}C & \theta_1 \\ & & \theta_2 \\ 0 \quad 0 & \frac{-\chi}{C_p} \quad 0 & \frac{-1}{C_p R} \end{bmatrix} \begin{bmatrix} h \\ \alpha \\ \dot{h} \\ \dot{\alpha} \\ v \end{bmatrix} + \begin{bmatrix} 0 \\ 0 \\ M^{-1}F_{2x1} \\ \\ 0 \end{bmatrix} \tag{2.51}$$

Where,

$$\theta_1 = \frac{I_\alpha \theta}{d} \quad , \; \theta_2 = \frac{-m_w x_\alpha b\theta}{d}$$

O= Null matrix , I=Identity matrix of [2x2]

[$M^{-1}k$] and [$M^{-1}c$] =Matrix of [2x2]

Solution is obtained by solving the simultaneous differential equations (equation 2.51) in MATLAB by ode45.

FLUTTER SPEED- By solving the equation matrix (a_3) we got a we have got five roots. The matrix *B(U)* has a set of five eigenvalues λ_i , $i = 1, 2, \ldots, 5$, which determine the stability of the trivial solution. We arrange these eigenvalues so that the first four are complex conjugates ($\lambda_2 = \lambda_1$ and $\lambda_4 = \lambda_3$). In the absence of the piezoelectricity effect, these eigenvalues are the same as those of the aeroelas- tic system. The fifth eigenvalue, which is always neg- ative, is a result of the electromechanical coupling. If the real parts of all eigenvalues are negative, the trivial solution is asymptotically stable. On the other hand, if one of the real parts is positive, the trivial solution is unstable. In addition, the real parts of these eigen- values represent the global damping and the positive imaginary parts correspond to the global frequencies of the piezoaeroelastic system. The speed for which one or more eigenvalues have zero real parts, corresponds to the onset of linear instability and is termed the flutter speed U_f.

Let

$\lambda 1 = a_1 + jb_1$, $\lambda 2 = a_1 - jb_1$

$\lambda 3 = a_2 + jb_2$, $\lambda 4 = a_2 - jb_2$

a_1 and a_2= Modal damping term

b_1 and b_2=Modal frequency term

As Free stream velocity(U) increases b_1 decreases and b_2 increases and at particular instant where, $b_1 = b_2$,the corresponding value of speed is called the flutter speed.

CHAPTER-3

EXPERIMENTAL ANALYSIS

This chapter explains the experimental analysis of the model starting from sample and piezoceramic material preparations and model analysis test set-up.

3.1 SAMPLE PREPRATION

(a) Brass shim

The brass shim is taken as a material used for conventional impact testing pieces available from Strength of Materials lab. It is finely finished by grinding, file and abrasive paper to make it prismatic. The dimension of brass shim are length 25mm, width 9.8 mm and thickness 1mm. Care is taken till the desired thickness is obtained uniformly during filing. The sample is mounted on a rigid robust steel plateat its base and steel plate is kept above the vibration shaker firmly so as to act as vibrating base for cantilever.

(b) BZT (Barium Zirconate titanate) material

BZT material is used to form piezoelectric shim. BZT stands here Barium Zirconate Titanate. There are following steps to prepare BZT:

1. First we take Barium carbonate, Calcium carbonate, Zirconium oxide and titanium oxide and blend these all with propanol for planetary milling. This process continues upto 11 hours and after that some powder is obtained which we have to dry.

2. After drying, grind the powder by the help of Agat Motor.

3. After grinding, Calcination of powder is required in the furnace at 1200^0C. It is used to remove carbonate and phase formation.

4. Now grind the powder into fine particles.

5. Now blend the powder with the Poly Vinyl Alcohol and dry the powder naturally.

6. Again grind the powder until finest particle is not obtained.

7. Pour that powder in a required shape die and press it.

8. After pressing, sinter the powder and put in furnace at 1300^0C, then it provides a final density and required micro structure and grain size. In present case circular disc piezo samples are prepared at ceramic engineering department.

9. In present case circular disc piezo samples are prepared at ceramic engineering department.

3.2 EXPERIMENTAL SET UP

The bimorph energy harvester presented in this section includes a tip mass. A bimorph piezoelectric cantilever is placed over a shaker with the help of rigid base. See Fig 3.1 the dimension of a shim material is 25x9.8x1 mm^3 and of piezo material is 20x9.8x1.8 mm^3.

The following set up is used for experiment-

1 Signal generator/ Function generator

2 Power Amplifier

3 Shaker (5N Indian make Shaker)

4 Digital oscilloscope

5 Piezoelectric accelerometer

Fig 3.2 shows the experimental setup.

Signal generators, also known variously as function generators, RF and microwave signal generators, pitch generators, digital pattern generators or frequency generators are electronic devices that generate repeating or non-repeating electronic signals (in either the analog or digital domains). A function generator is a device which produces simple repetitive waveforms. Such devices contain an electronic oscillator, a circuit that is capable of creating a repetitive waveform. In present case, a signal generator producing sine wave form is employed.

An electronic amplifier, amplifier, or (informally) amp is an electronic device that increases the power of a signal. It does this by taking energy from a power supply and controlling the output to match the input signal shape but with a larger amplitude. In this sense, an amplifier modulates the output of the power supply and amplitude of sine wave is maintained constant throughout experiment.

The electrodynamics shaker functions to deliver a force proportional to the current applied to its voice coil (see sidebar). These devices are used in such diverse activities as product evaluation, stress screening, squeak-and-rattle testing and modal analysis. These shakers may be driven by sinusoidal, random or transient signals based upon the application. They are invariably driven by an audio-frequency power amplifier and may be used "open loop" (as in most modal testing) or under closed-loop control where the input to the driving amplifier is servo-controlled to achieve a desired motion level in the article under test. In present case, a mini 5N shaker is used.

Figure3.1Bimorph Piezoelectric cantilevered Beam with Tip Mass

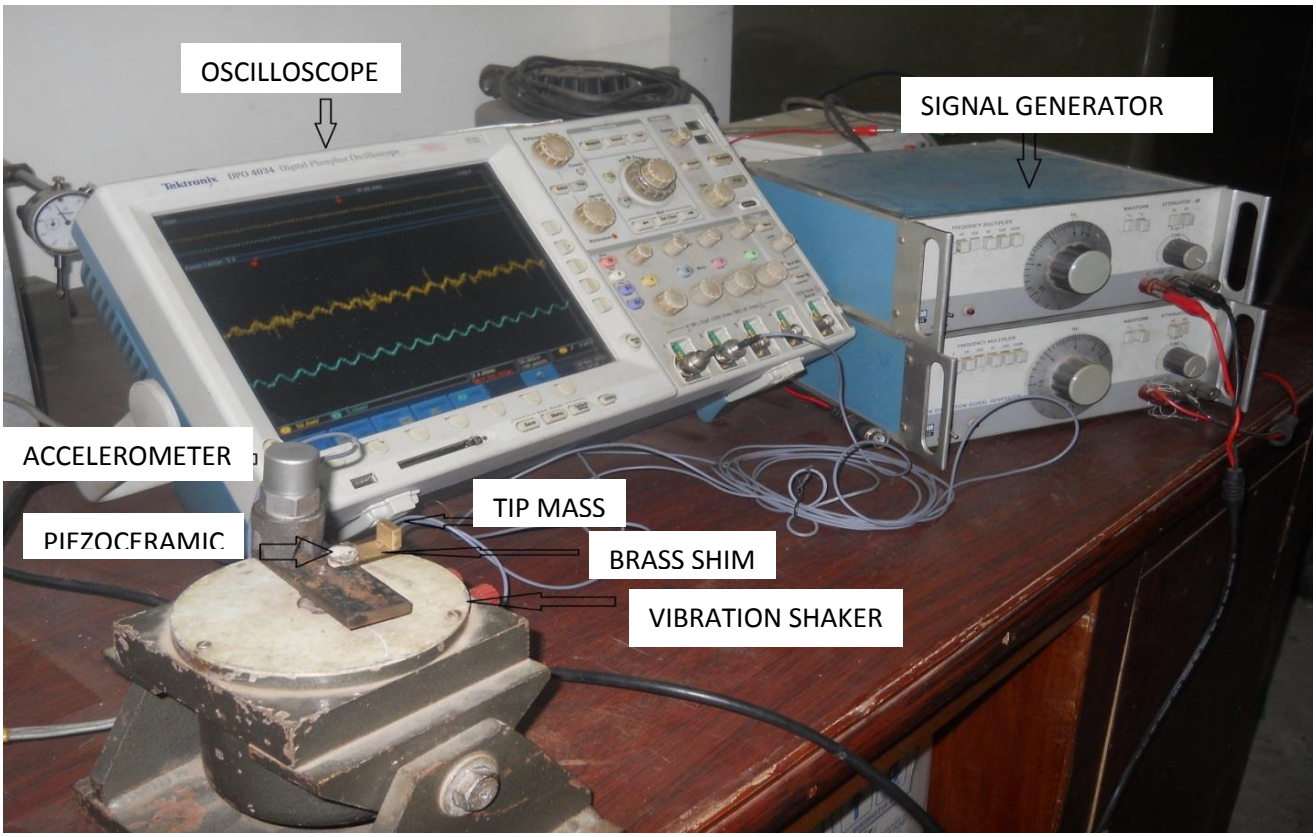

Figur.3.2Experimental set up of Bimorph Piezoelectric Cantilevered Beam

Oscilloscopes are commonly used to observe the exact wave shape of an electrical signal. Oscilloscopes are usually calibrated so that voltage and time can be read as well as possible by the eye. This allows the measurement of peak-to-peak voltage of a waveform, the frequency of periodic signals, the time between pulses, the time taken for a signal to rise to full amplitude(rise time), and relative timing of several related signals. In present case, a digital oscilloscope (Tecktronix make) is used and 2 channels are employed; one for input sine wave signal checking and other for output voltage obtained from piezoceramic layer (see Fig. 3.3). The oscilloscope has feasibility to record digital data in excel sheet as well as to save the screen shot whenever needed.

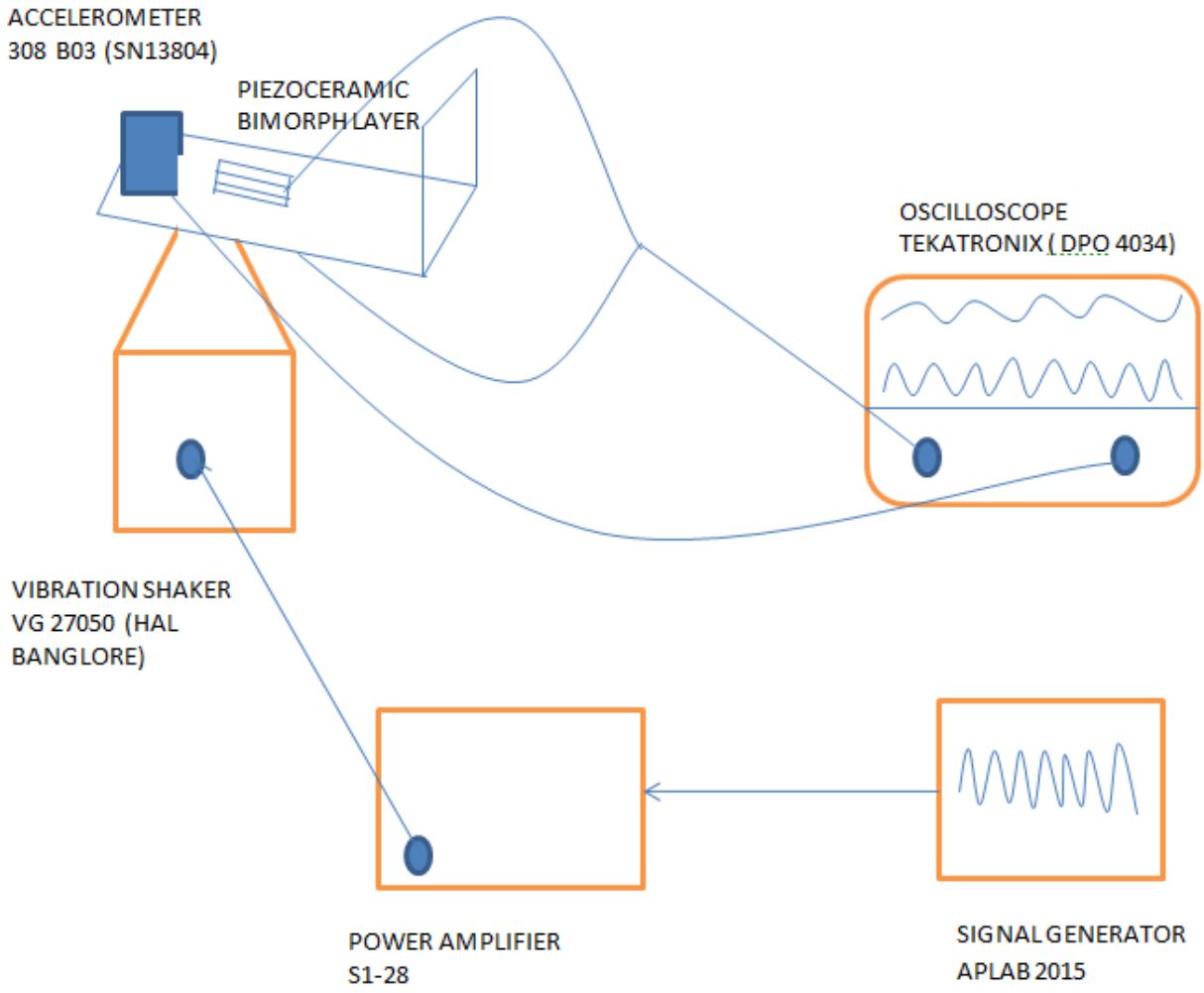

Fig3.3 Block Diagram of Experimental Set-up

3.3 SINE SWEEP TEST

Sine sweep test is used to find the natural frequency of the structure and finding out the corresponding amplitude by sweeping out the frequency. The base of physical model of bimorph piezoelectric cantilever is fixed over the vibration shaker. The shaker is made to vibrate harmonically over a suitable frequency steps. It vibrates initially at low frequency and step by step to largest frequency provided. An accelerometer is mounted over the base of cantilever whose output cable goes into the Oscilloscope to measure the input force history. The frequency

is varied from a signal generator via the power amplifier which provides the force to vibration shaker. One lead from the surface of piezoelectric element goes into the Oscilloscope in channel 2. Now the magnitude of piezoceramic output voltage is recorded for different frequency steps and finally with help of frequency response generated, we find out the natural frequency of the system. The peak obtained is the natural frequency of the cantilever. When the excitation frequency matches with this natural frequency then resonance occurs, and the maximum amount of voltage is obtained at this resonance condition. Thus, output voltage is proportional to the amplitude.

CHAPTER-4

FINITE ELEMENT ANALYSIS

This chapter presents the solid modeling and meshing of Piezoelectric bimorph cantilever model. This chapter also describes the type of element used for modeling.

4.1 SOLID MODELLING OF CANTILEVER WITH TIP MASS

Compared with the traditional analytical modeling of a PCB generator, finite element analysis (FEA) is a more tractable approach to predicting he dynamic response of a harvester. Further, for the design of MEMS-scale piezoelectric energy harvesters, the prototype fabrication and laboratory testing generates big challenges and difficulties during the process. In this section, based on the work given in Zhang and Williams[2010B] , the use of FEA to study the dynamic response of a PCB generator subjected to a harmonic excitation is presented. The FEA simulation was performed using ANSYS.14 and is compared against experimental results, in terms of both the PCB tip displacement and the induced electrical potential of the PCB generator. A solid model of the beam is created in ANSYS with various element included.

4.2 PIEZOELECTRIC ANALYSIS IN ANSYS

The linear constitutive equation for the piezoelectric materials can be expressed as follows,

$$[\sigma] = [s^E]\{S\} + [d]^t\{E\}$$
$$[D] = [d]\{S\} + [\varepsilon^T]\{E\}$$

Where {σ} and{S} are the stress and strain vectors, respectively (six components x, y, z, yz, xz, xy);{D} and {E} are the electrical displacement vector and the electrical field vector,

respectively (three components x, y, z) ; $[s^E]$ is the six by six compliance matrix evaluated at constant electric field; i.e. short circuit; $\{d\}^T$ is a piezoelectric constant matrix; and $[\varepsilon^T]$ is a three by three dielectric matrix evaluated at constant stress. The superscript E represent the data measured under constant electric field i.e. PZT electrodes under short circuit condition, and superscript T represent the data under constant stress.

As mentioned previously, piezoelectric material exhibits strong electromechanical energy. Consequently, FEA of such device requires the use of multi-physics package. For orthotropic materials, the flexibility or compliance matrix[S] and piezoelectric strain matrix [d] can be expressed as:

Flexibility Matrix(Stiffness Matrix), $[s] = \begin{bmatrix} S_{11} & S_{12} & S_{13} & & & \\ & S_{11} & S_{13} & & & \\ & & S_{33} & & & \\ & & & S_{44} & & \\ & & & & S_{55} & \\ & & & & & S_{66} \end{bmatrix}$

Relative Dielectric Matrix, $[\varepsilon^s] = \begin{bmatrix} \varepsilon_{11} & & \\ & \varepsilon_{22} & \\ & & \varepsilon_{33} \end{bmatrix}$

The finite elements in ANSYS that can be used to model the piezoelectric devices include SOLID185, SOLID5 and CIRCU94 and the specific descriptions of these elements can be found in the ANSYS theory manual. SOLID5 has a 3-D magnetic, thermal, electric, piezoelectric, and structural field capability with limited coupling between the fields. The element has eight nodes with up to four degrees of freedom(Ux, Uy, Uz and V) at each node. Scalar potential formulations (reduced RSP, difference DSP, or general GSP) are available for modeling

magnetostatic fields in a static analysis. When used in structural and piezoelectric analyses, SOLID5 has large deflection and stress stiffening capabilities. SOLID45 is used for the 3-D modeling of solid structures. The element is defined by eight nodes having three degrees of freedom at each node: translations in the nodal x, y, and z directions. The element has plasticity, creep, swelling, stress stiffening, large deflection, and large strain capabilities. CIRCU94 is a circuit element for use in piezoelectric-circuit analyses. The element has two or three nodes to define the circuit component and one or two degrees of freedom to model the circuit response. CIRCU94 is applicable to full harmonic and transient analyses. The above Fig.4.1 shows a bimorph piezoelectric model having a tip mass at the end.

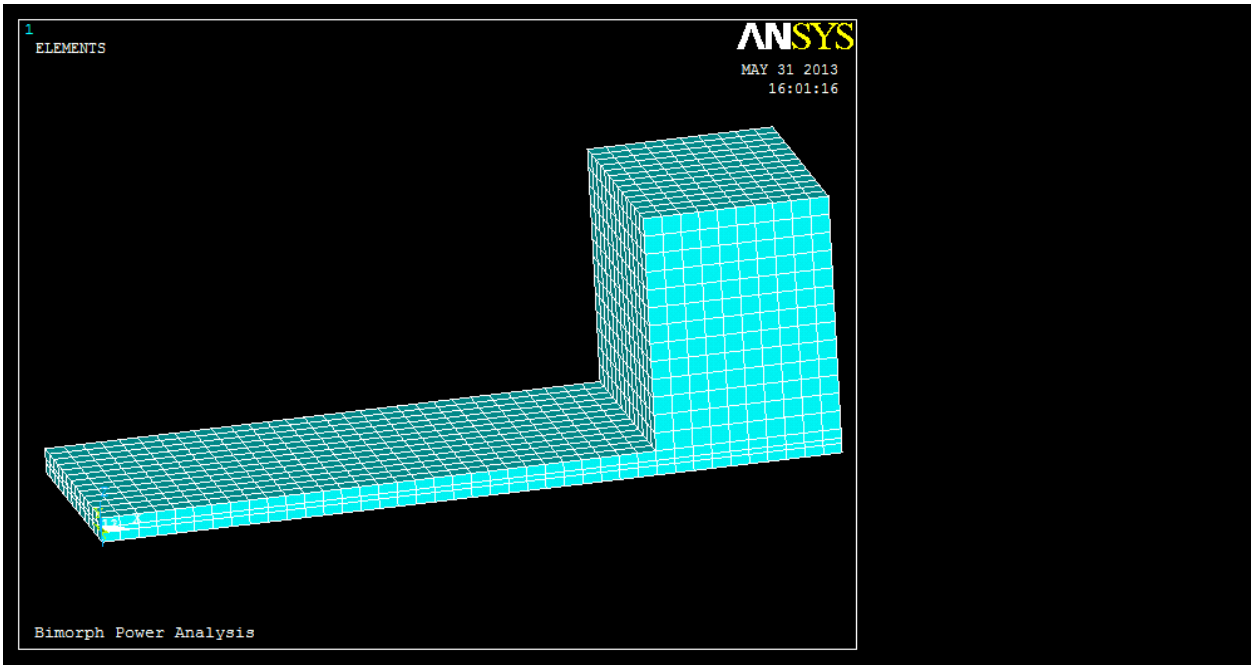

FIGURE 4.1: Solid Model of Piezoelectric cantilevered Beam with Meshing

The material of the shim and tip mass is brass material and the material used for Piezoelectric shim is a PZT (Lead Zirconate Titanate). This model is prepared in ANSYS by the use of APDL commands..

4.3 ELEMENTS USED FOR DISCRITIZATION WITH CONSTRAINTS AND LOADS

The Fig4.2 shows the model is meshed.

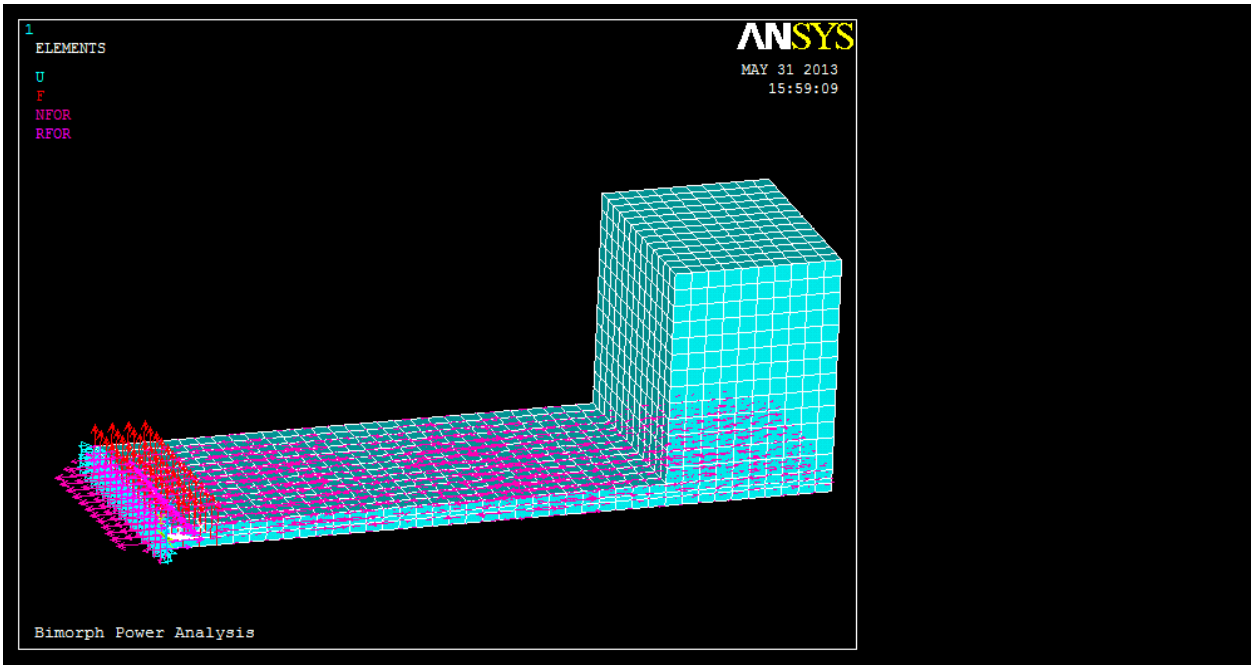

Figure4.2 Meshed model of Cantilever Piezoelectric Beam

The size element of this meshing is 5e-4 to create a fine mesh. After meshing the nodes are generated. The following mesh details are observed,

Mesh element Size = 5e-4 mm

Total number of elements generated = 3250

Number of elements for piezoceramic (SOLID5) = 520 (For top and Bottom)

Number of elements for Shim(SOLID185) = 520

Number of elements for Tip Mass =1690

Total number of nodes Created = 4298

CHAPTER-5

RESULTS AND DISCUSSIONS

The following chapter describes the results of all models described above by the use of MATLAB and ANSYS software . The results are followed by an experiment conducted on a piezoelectric cantilevered bimorph model in a laboratory.

5.1 DISTRIBUTED PARAMETER MODEL

Even distributed parameter models are reliable, they are computationally cumbersome. Exact solutions are difficult to obtain, however, approximate methods like Galerkin's approach can be used to get their solutions. Lumped parameter models leads to ordinary second order differential equations and give more or less several similar insights as those obtained from distributed parameter models.

MATLAB CODE WITH RK SOLVER-

```
--------------------------------------------------------------------------------
syms u x fux ful phib T Q1
mt=0.03375e-3; l=20e-3;b=6.4e-3;
ts=0.14e-3;tp=0.26e-3;Es=100e9;
Ep=66e9;rhs=8700;rhp=7800;
d31=190e-12;e=Ep*d31;
ys=(ts/2);%neutral axis distance of substrate
yp=((ts/2)+tp);%neutral axis distance of piezo
Is=(b*ts^3/12);
Ip=(b*tp^3/12);
EI=Es*(b*ts^3/12)+2*Ep*b*((tp^3/12)+tp*((tp+ts)/2)^2);
rhoA=b*(rhs*ts+2*rhp*tp);
alp=mt/(rhoA*l);
freq=('1+cos(u)*cosh(u)+0.05*u*(cos(u)*sinh(u)-sin(u)*cosh(u))');%alp=0.05 by the calculation frm column 18
u=solve(freq,u);
omega=sqrt(EI/(rhoA*l^4)*u^4);
disp(eval(omega/(2*pi)));
A=1-sin(u)*sinh(u)+cos(u)*cosh(u)-2*u*alp*sin(u)*cosh(u); B=-2*u*alp*cos(u)*cosh(u)-(sin(u)*cosh(u)+cos(u)*sinh(u));
C=1+sin(u)*sinh(u)+cos(u)*cosh(u)+2*u*alp*cos(u)*sinh(u); D=2*u*alp*cos(u)*cosh(u)+(sin(u)*cosh(u)+cos(u)*sinh(u));
v=u/l;%v=beta
fux=A*cos(v*x)+B*sin(v*x)+C*cosh(v*x)+D*sinh(v*x);
ful=A*cos(v*l)+B*sin(v*l)+C*cosh(v*l)+D*sinh(v*l);
X=int(fux^2,0,l);
```

```
Y=rhoA*X;
m=alp*rhoA*l;
Z=m*(omega*ful)^2;
BA=sqrt(1/(Y+Z));
phib=BA*fux;
phibl=BA*ful;
Q1=-v^2*A*cos(v*x)-v^2*B*sin(v*x)+v^2*C*cosh(v*x)+v^2*D*sinh(v*x);%double differentiation of fux
T=BA*Q1;%double differentiation of phib
M=rhs*b*ts*int(phib^2,0,l)+2*rhp*b*tp*int(phib^2,0,l)+(mt*phibl^2);
K=(Es*Is+2*Ep*Ip)*int((T)^2,0,l);
Jp=(e/2*tp)*b*((tp+(ts/2))^2-(ts/2)^2);
THETA=Jp*int(T,0,l);
c=2*0.01*sqrt(K*M);
Cp=(l*b*e)/(2*tp);
R=10;%ohm h=1e-10;
A=[0,1,0;(-K/M),(-c/M),(THETA/M);0,(-THETA/Cp),(-1/Cp*R)];
x1=0;x2=0;x3=0;
X=[x1;x2;x3];
T=1e-7;
i=1;
for t=0:h:T
   Y(:,i)=X;
   Da=[0,-B*omega^2*sin(omega*t),0]';  Db=[0,-B*omega^2*sin(omega*(t+h/2)),0]';
   Dc=[0,-B*omega^2*sin(omega*(t+h)),0]';
   K1=h*(A*X+Da);     K2=h*(A*(X+(K1/2))+Db);
    K3=h*(A*(X+(K2/2))+Db);    K4=h*(A*(X+K3)+Dc);
    X=X+(1/6)*(K1+2*K2+2*K3+K4);
    i=i+1;
end
ti=[0:h:T];
plot(ti,Y(2,:)');
```

All the results are obtained by solving the differential equation by RK Solver developed in MATLAB. The result obtained for a distributed parameter model shows that the voltage obtained is very small in amplitude. So the power obtained is very small. As we provide sinusoidal base excitation to base, so the response of displacement and voltage comes in sinusoidal manner.

Fig5.1 shows the variation of displacement with time , Fig5.2 shows that variation of voltage with time and Fig5.3 shows the variation of power with time. From Fig5.1 and Fig5.2 the maximum amount of displacement at free end of cantilever is 4e-3 meters and the maximum amount of voltage is 2e-15 volt. From Fig5.3 the amount of power harvested is very less which is only 1.8 e-33 watts.

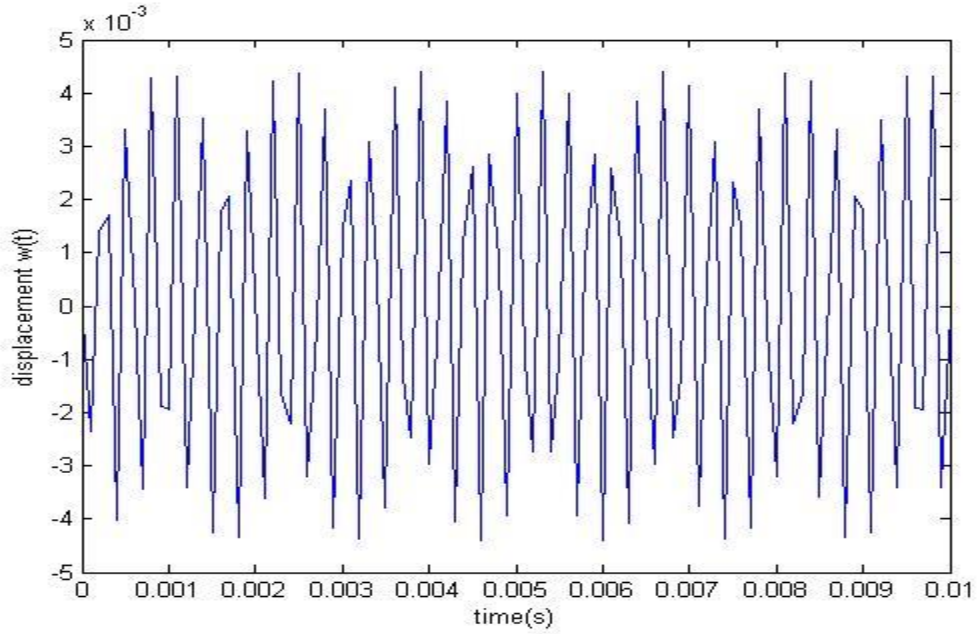

Fig5.1 Variation of Displacement with time

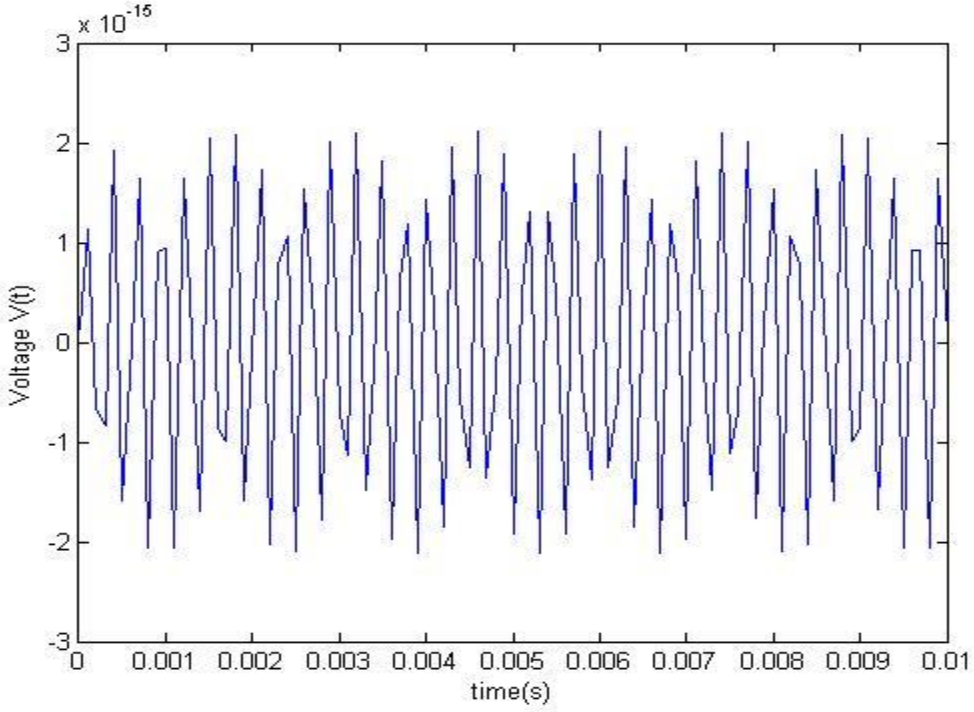

Fig5.2 Variation of Voltage with time

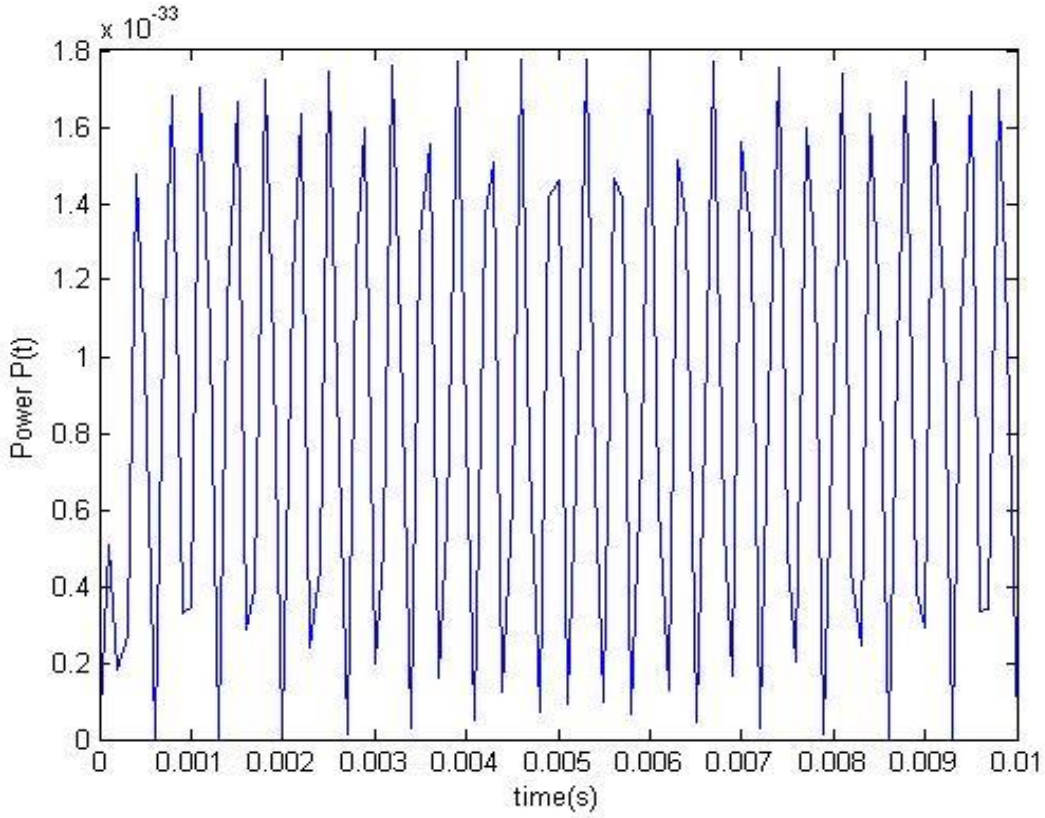

Fig5.3 Variation of Power with time

5.2 LUMPED PARAMETER MODEL

Data used for Simulation-

Table-1 Dimensions and properties of cantilever [20]

Parameter	Substrate (s)	Piezoelectric (p)
Beam length(L),(mm)	20	20
Beam width(w),(mm)	6.4	6.4
Thickness t,(mm)	0.14	0.26
Elastic Modulus c,(GPa)	100	66
Densities,(kg/m^3)	8700	7800
Piezoelectric Constant,d_{31}(m/V)	---	180e-12
Absolute permittivity ε_{33}^S	---	15.93nF/m
Electromechanical coupling term, θ	---	3.1623e-5

(a) SINGLE DEGREE OF FREEDOM-

Single Degree of Freedom

```
clc
clear all
lb=20e-3; wb=6.4e-3;
rhos=8700;rhop=7800;
tht=3.1623e-5; ts=0.14e-3; tp=0.26e-3;
Es=100e9; Ep=66e9; mt=.03375e-3;
R=10;%resistance
zet=.01; eps=15.93e-9;
rhoA=wb*(rhos*ts+rhop*tp); mb=rhoA*lb;
m=mt+(33/140)*mb;
EI=Es*(wb*ts^3/12)+2*Ep*wb*((tp^3/12)+tp*((tp+ts)/2)^2); K=3*(EI)/(lb^3);
omgn=sqrt(K/m);
c=2*zet*sqrt(K*m);%damping c0-efficent cp=(lb*wb*eps)/(2*tp);
ub=1;%base acceleration=B in previous program
k=2;
for omg=0.8*omgn:1.2*omgn
   num=(i*omg^3*tht*ub*m);
   den=(((K-m*omg^2)+i*c*omg)*(i*cp*omg+(1/R)))+(i*omg*tht^2);
   V(k)=abs(num/den);
   k=k+1;
end
omge=(0.8*omgn:1.2*omgn);
plot(omge/(2*pi),V);
xlabel('\omega (Hz)'); ylabel('Induced voltage (V)');
```

In a single degree of freedom model, the piezoelectric bimorph model is considered as an element of mass, stiffness and damping. Fig5.4 shows the variation of displacement with natural frequency, Fig 5.5 shows the variation of voltage with resistance and Fig5.6 shows the variation of power with resistance. From the Fig5.4 and Fig5.5 we observe that the output comes for a very small frequency range i.e. frequency bandwidth is very narrow. If we deviate a little bit from this frequency range then harvested power is going to decrease. For a very narrow bandwidth the amount of power harvested is very less. This model only produces a small amount of power which is not effective for implementation. As from Fig5.4 the displacement is 5e-4 and from the Fig5.5 the amount of voltage generated 10 volt. From the Fig 5.6 the power harvesting from the single degree of freedom model is 1e-3 watt.

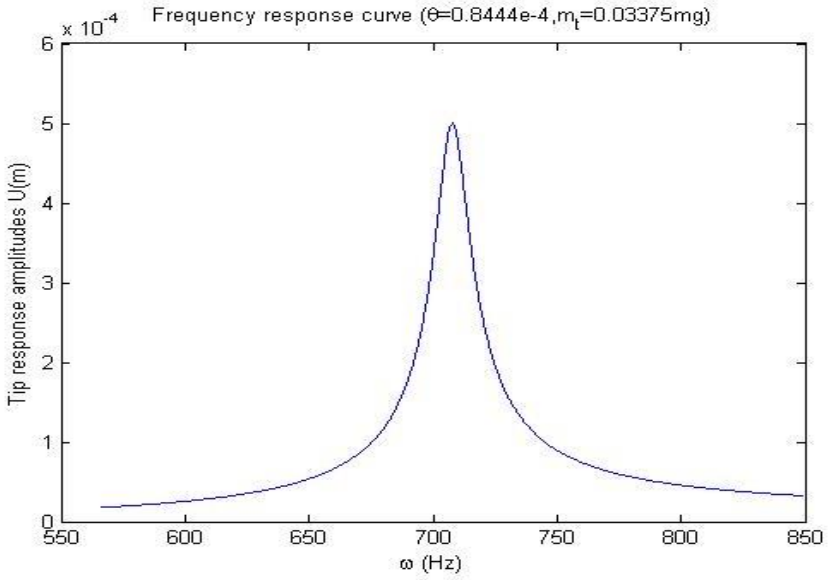

Fig5.4 Displacement Variation With natural Frequency

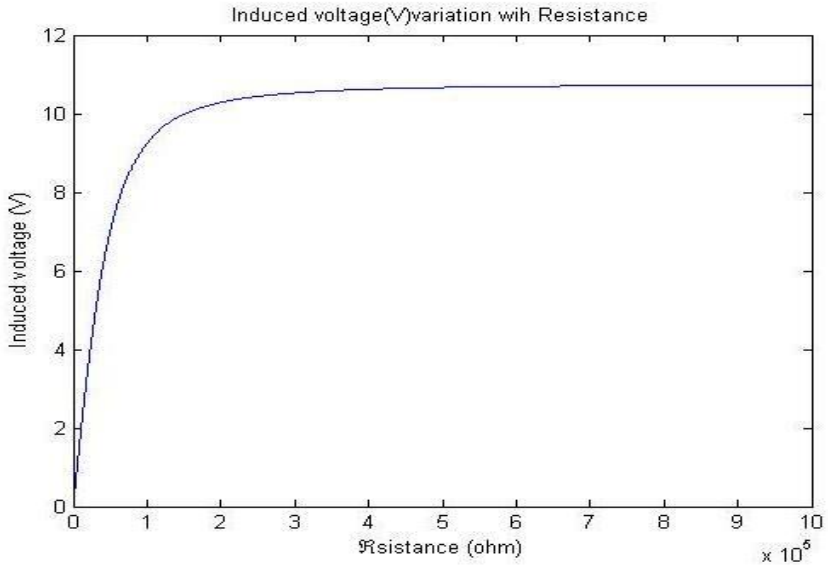

Figure5.5 Voltage Variation with Resistance

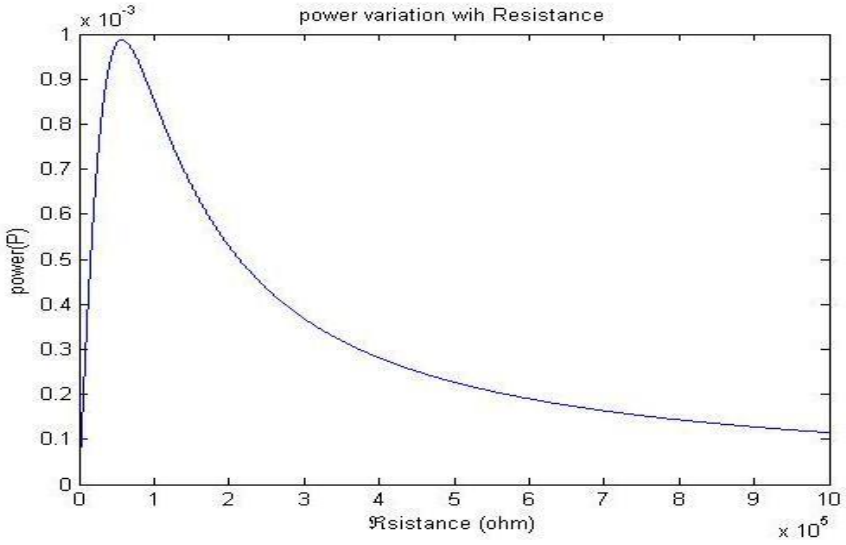

Figure5.6 Power variation with Resistance

(b) TWO DEGREE OF FREEDOM MODEL

Matlab Code

```
lb=20e-3;  wb=6.4e-3;  rhos=8700;  rhop=7800;  tht=3.1623e-5;  ts=0.14e-3;
tp=0.26e-3;  Es=100e9;  Ep=66e9;  mt=0.03375e-3;  zet=0.01;  eps=15.93e-9;
rhoA=wb*(rhos*ts+2*rhop*tp);     mb=rhoA*lb; m=mt+(33/140)*mb;
EI=Es*(wb*ts^3/12)+2*Ep*wb*((tp^3/12)+tp*((tp+ts)/2)^2);  K=3*(EI)/(lb^3);
omgn=sqrt(K/m);   c=2*zet*sqrt(K*m);%damping c0-efficent
cp=(lb*wb*eps)/(2*tp);  ub=0.00001;  mew=0.1;  alp=0.8;  mm=mew*m;
omgna=alp*omgn;    kk=omgna^2*mm;  zet2=0.002;  cc=2*zet2*sqrt(kk*mm);
k=1;
R1=10;%resistance
for omg=0.4*omgn:1.6*omgn
  R=R1;
   num=(((i*cc*omg+kk)*mm*omg^2)+(m*omg^2*(-mm*omg^2+i*cc*omg+kk)))*(i*omg*cp+(1/R))*ub;
   den=((-mm*omg^2+i*cc*omg+kk)*(-m*omg^2+i*c*omg+K)-
(i*cc*omg+kk)*mm*omg^2)*(i*omg*cp+(1/R))+(i*tht^2*omg)*(-mm*omg^2+i*cc*omg+kk);
   U1(k)=abs(num/den);     A=((i*tht*omg)/(cp+(1/R)));     V1(k)=abs(A*U1(k));     P1(k)=V1(k)^2/R;     k=k+1;
end
k=1;
R2=30;%resistance
for omg=0.4*omgn:1.6*omgn
  R=R2;
   num=(((i*cc*omg+kk)*mm*omg^2)+(m*omg^2*(-mm*omg^2+i*cc*omg+kk)))*(i*omg*cp+(1/R))*ub;
   den=((-mm*omg^2+i*cc*omg+kk)*(-m*omg^2+i*c*omg+K)-
(i*cc*omg+kk)*mm*omg^2)*(i*omg*cp+(1/R))+(i*tht^2*omg)*(-mm*omg^2+i*cc*omg+kk);
   U2(k)=abs(num/den);     A=((i*tht*omg)/(cp+(1/R)));     V2(k)=abs(A*U2(k));     P2(k)=V2(k)^2/R;
   k=k+1;
end
omga=[0.4*omgn:1.6*omgn];
figure(1);
plot(omga/(2*pi),U1,'-.',omga/(2*pi),U2,'.-',omga/(2*pi),U3);
xlabel('\omega (Hz)');   ylabel('Tip response amplitudes U_1(m)');
title('Frequency response curve (\mu=0.7 and \alpha=0.8 and \zeta 2=.009)');  legend('R=10 ohms','R=30 ohms','R=50 ohms')
figure(2);
plot(omga/(2*pi),V1,'-.',omga/(2*pi),V2,'.-',omga/(2*pi),V3);
xlabel('\omega (Hz)');  ylabel('Induced voltage (V)');
title('Frequency response curve (\mu=0.7 and \alpha=0.8 and \zeta 2=.009)');  legend('R=10 ohms','R=30 ohms','R=50 ohms')
figure(3);
plot(omga/(2*pi),P1,'-.',omga/(2*pi),P2,'.-',omga/(2*pi),P3);
xlabel('\omega (Hz)');   ylabel('power(W)');
title('Frequency response curve (\mu=0.7 and \alpha=0.8 and \zeta 2=.009)');  legend('R=10 ohms','R=30 ohms','R=50 ohms');
```

As the power harvested in single degree of freedom model is very small due to very narrow bandwidth so two degree of freedom model is used for generation of great amount of power by increasing the bandwidth of the peak amplitude. Maximum power generates at resonant condition which is harmful for harvester. In one degree of freedom model the energy is harvested only at resonant condition, if we deviate from this resonant condition the power is not harvested

properly but two degree of freedom model allow us to harvest power rather than resonant condition.

Fig 5.7 and Fig 5.10 shows the variation of displacement with natural frequency, Fig 5.8 and Fig 5.11 shows the variation of voltage with natural frequency and Fig 5.9 and Fig 5.12 shows the variation of power with natural frequency with different μ values.

In order to illustrate the outputs of the model, the dimensions and properties of bimorph-harvester considered here are depicted in Table1. The other constant parameters considered are: tip-mass m_t=0.03375 mg, system damping ratio ξ=0.01 and the base acceleration U_b=0.1 mm/s^2.

As we see that, as we decrease the value of μ the peak is going to closer and trying to merge as one peak, this condition show the maximum energy is harvested from harvester. So we conclude that two degree of freedom model gives the maximum amount of energy if else we deviate from the resonant condition. All the routine is implemented in MATLAB program. The natural frequency of the system is found to be 720.7 Hz, which is very close to that obtained from one-mode distributed parameter model.

(a) Variation of parameters with μ=0.05, α= 0.92 ξ_2=0.002

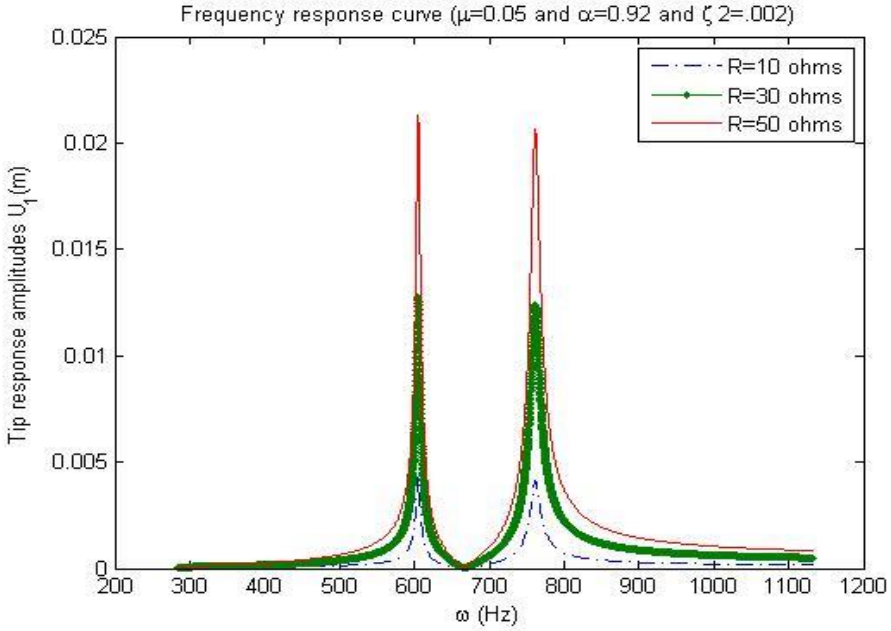

Figure 5.7 Displacement variation with natural frequency

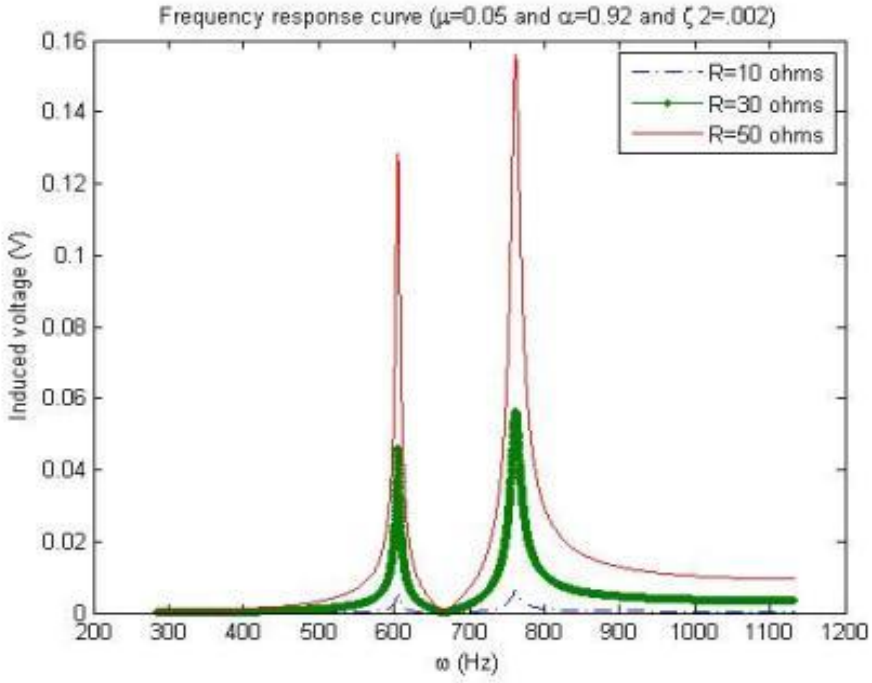

Figure5.8 Voltage variation with natural frequency

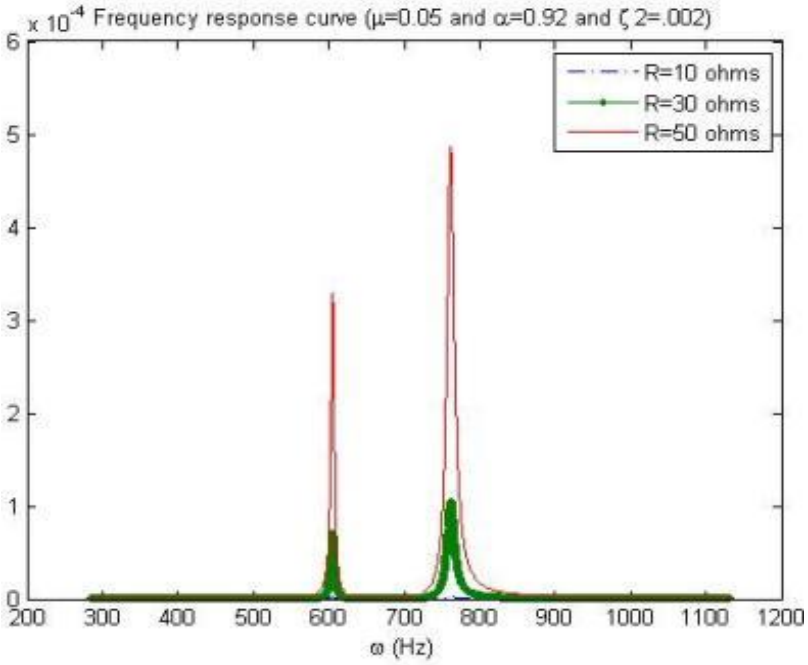

Fig5.9 Power variation with natural frequency

(b)Variation of Parameters with μ=0.01, α= 0.92 ξ_2=0.00

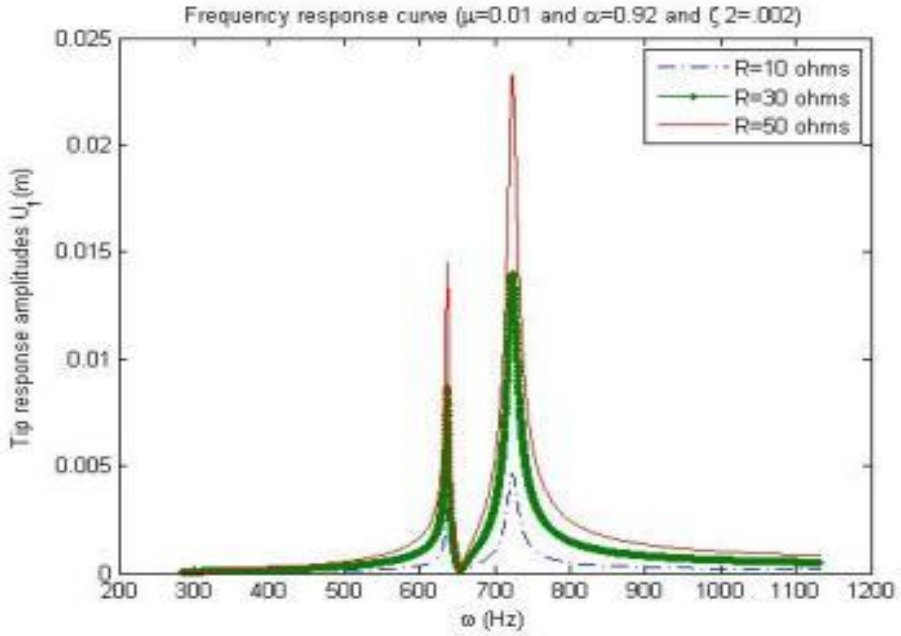

Figure5.10 Displacement variation with natural frequency

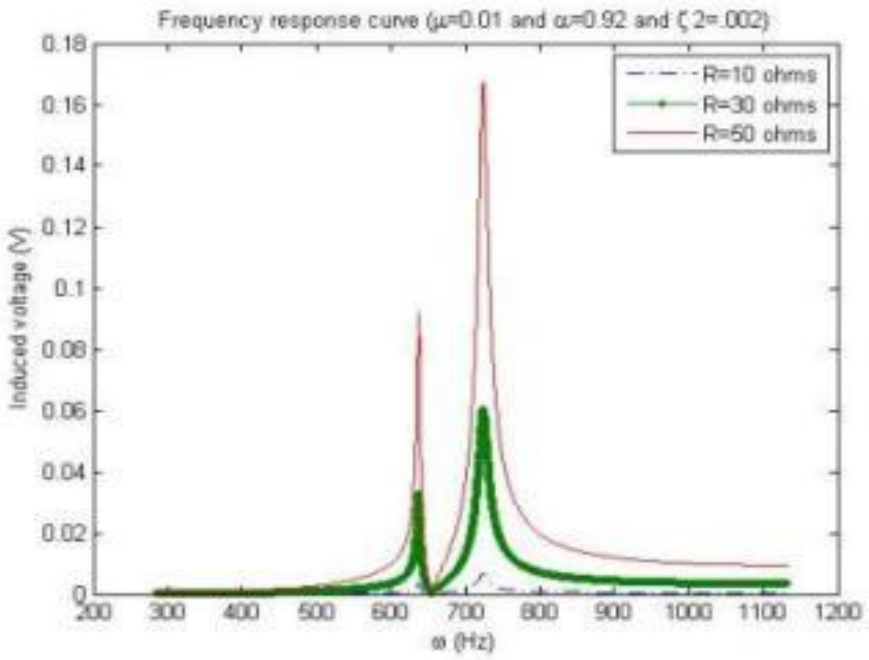

Figure 5.11 Voltage variation with natural frequency

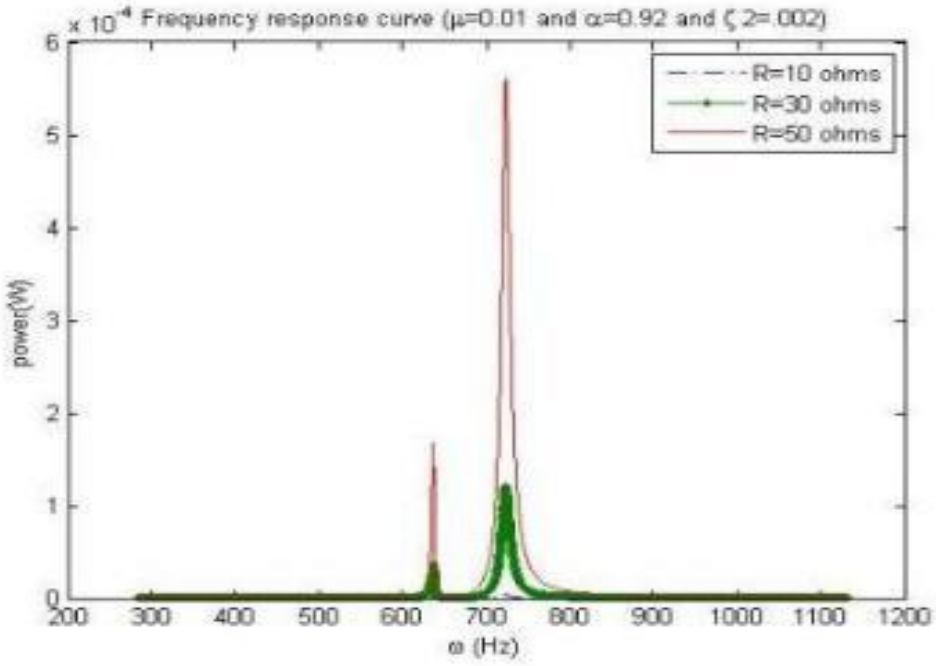

Figure.5.12 Power variation with natural frequency

SUITABLE SELECTION OF α VALUE

As we know that when the two peaks comes close to each other within the frequency domain then maximum amount of power is harvested. So we have to select the optimal value of **α** with variation of **μ** which provides the maximum amount of power harvested. So we studied three cases for different value of **α**-

(I) When **α >1**

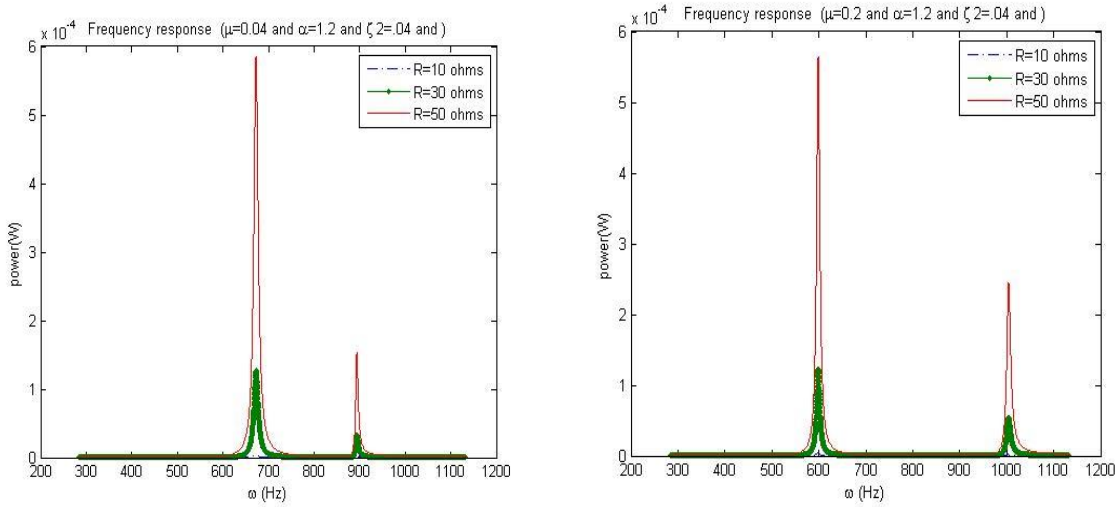

Figure 5.13 Variation of power with natural frequency

(II) When **α=1**

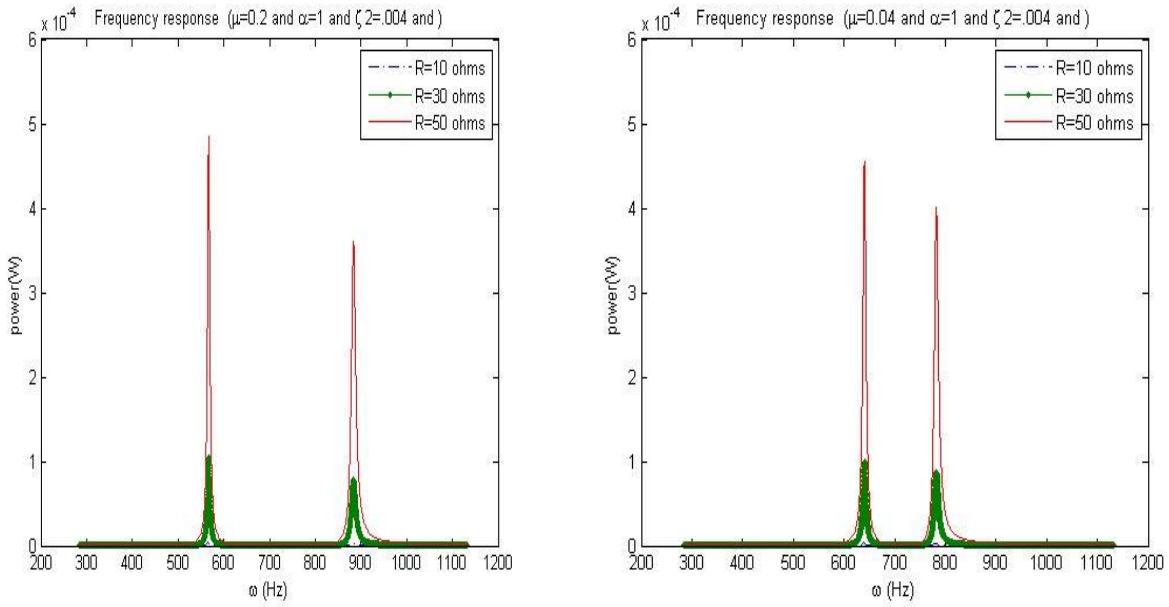

Figure 5.14 Variation of power with natural frequency

(III) When $\alpha<1$

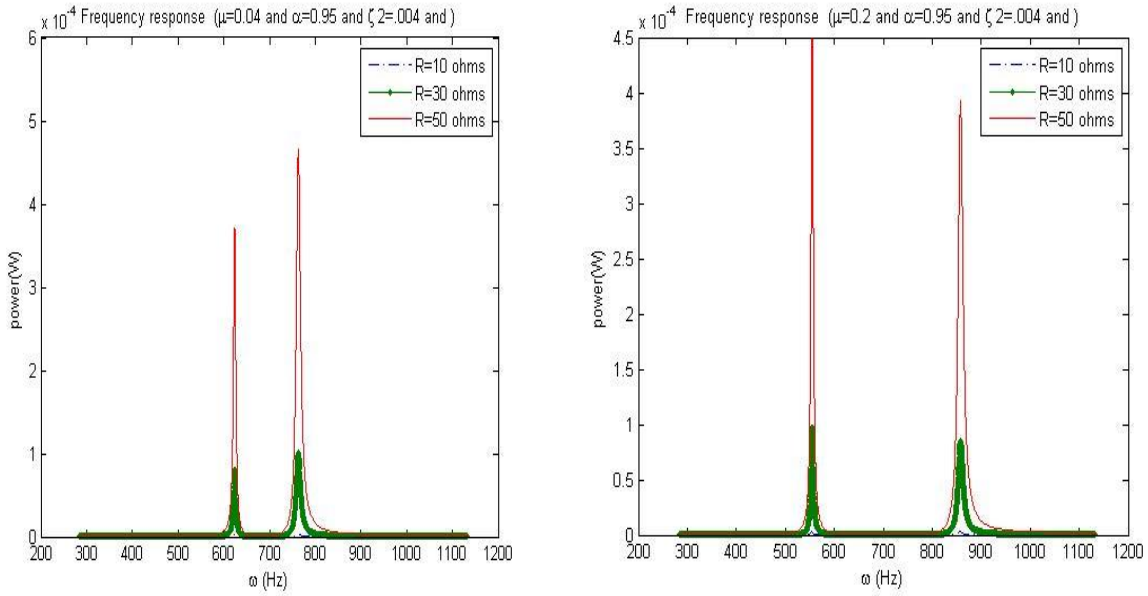

Figure 5.15 Variation of power with natural frequency

As we seen from the fig 5.13, Fig 5.14 and Fig 5.15 as we decrease the μ value the first peak is decreasing and other peak is increasing. We finally conclude that the two peaks are much closer

when α<**1** for a small value of μ**.** So for maximum energy harvesting we have to choose α less than one.

5.3 PIEZOAEROELASTIC MODEL

Table-I shows the data for analysis. The airfoil cross-section and coupling terms are selected from Ref [30].

Table-2 Simulation Parameters for an Aero-elastic System

PARAMETERS	VALUE	PARAMETERS	VALUE
A	-0.6719	B	0.1905 meter
c_α	0.016 m^2/sec	c_h	27.43 kg/sec
$c_{l\alpha}$	6.757	$c_{m\alpha}$	0
I_α	$m_w x_\alpha^2 b^2 + 0.009039$ kg/m2	k_α	$12.77 + (1003 x_3^2)$ N-m
k_h	2844.4 N/m	m_t	15.52 kg
m_w	4.34 kg	x_α	-(0.0998+a)
ρ (density of air)	1.225`kg/m3	Resistance(R)	1 Mohm

The matrix [A] has a set of five eigenvalues. The first four are similar to those of a pure aeroelastic system in the absence of the piezoelectricity effect. The fifth eigenvalue is a result of the electromechanical coupling. This fifth eigenvalue is always real negative as in the case of piezoelectric systems subjected to base excitations. The first four eigenvalues are complex conjugates. The real part of these eigen values represent the damping co-efficient and positive imaginary part corresponds to a global natural frequencies of the piezoaeroelastic system. Because λ_5 is always real negative the stability of the trivial solution depends upon the only first four Eigen values. The speed at which either first and third or second and fourth Eigen values are same is called the flutter speed. Fig5.17(a) and Fig5.17(b)show the variation of voltage and power respectively with the time. These are obtained by solving the equation (2.3.7) in MATLAB by ODE(45) and we got a variation of power and voltage with respect to time**.**

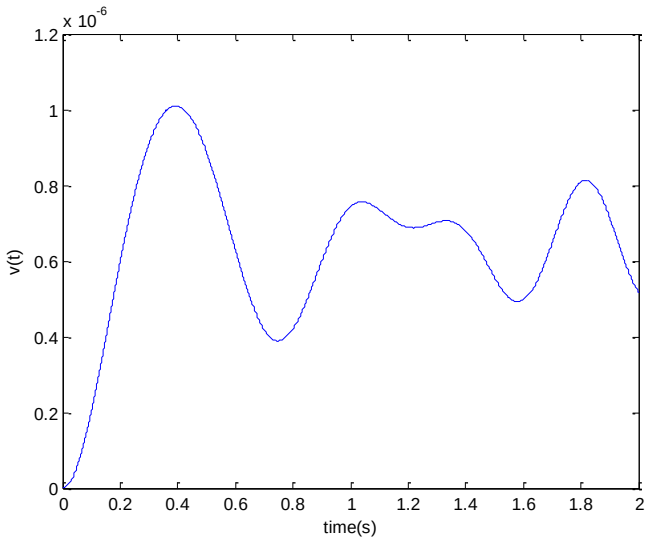

Fig5.16- Variation between voltage and time at Time(sec) at x_α=0.25 and Flutter speed=6.26m/sec

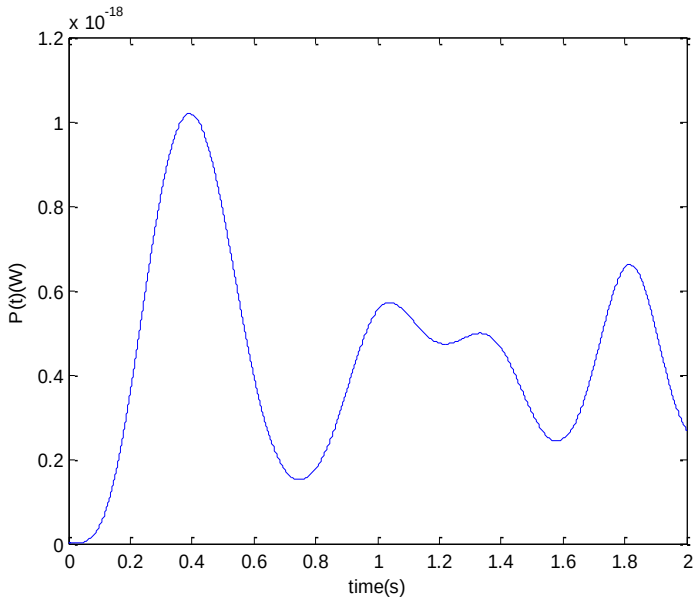

Fig5.17 Variation between Power and time at x_α=0.25 and Flutter speed=6.26m/sec

Optimization Parameter for Flutter speed

As we know that the maximum amount of power is harvested at low flutter speed so we have to optimize the parameters to get minimum flutter speed. Flutter speed is a speed at which instabilities occurs in the system it means system goes to unstable state. If we use higher speed there is more instabilities occur in the system which causes the system to remain permanently in unstable system i.e. it is very difficult for the system to return back into the stable state. The flutter is not continuous in system because it is dependent on the wind speed.

Fig 5.18 shows the variation of flutter speed with eccentricity, Fig 5.19 shows the variation of flutter speed with K_h (stiffness constant for plunge) and Fig 5.18 shows the variation of flutter speed with k_α (stiffness constant for pitch).

Our aim is to find out the minimum value of flutter speed with variation of parameter so finally we have to select the optimize parameters for maximum amount of energy harvesting. As we see that from the Fig 5.18, at lower eccentricity the flutter speed is lower but after some specific value (i.e. 0.3) the flutter speed is going to increase rapidly for a specific range (upto 0.4) and then after there is a very slight variation in flutter speed with increase in eccentricity . Similarly from the Fig5.19 and Fig5.20 we select the optimum value of K_h and k_α to get minimum amount of flutter spped. As we know that from the above theory the maximum power is harvested at lower flutter speed i.e. the lower flutter speed is obtained at low value of eccentricity between elastic axis and centre of mass. As from Fig5.18, Fig 5.19 and Fig5.20 we also conclude that the lower amount of flutter speed is obtained at some particular value, now we select those values for the calculation purpose to find out the voltage and power from the system.

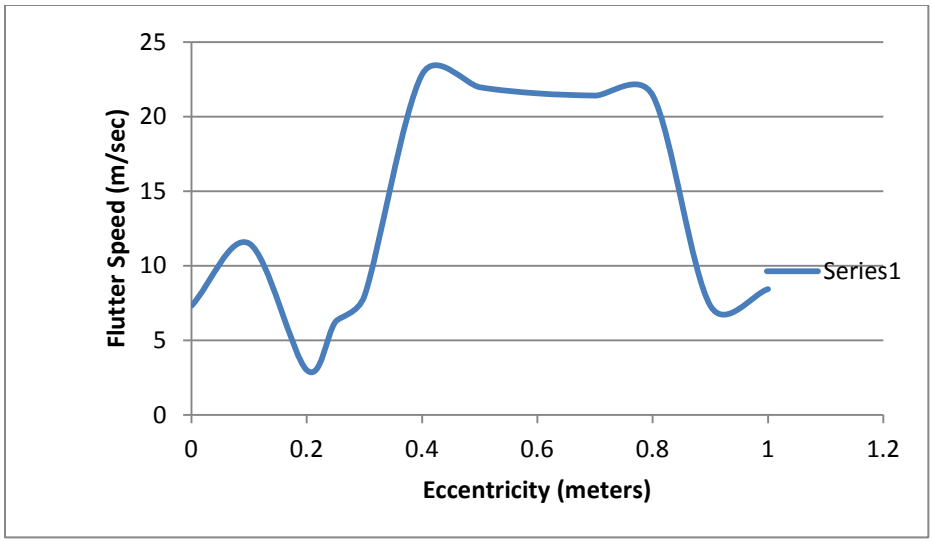

Figure-5.18 (variation between Flutter speed and eccentricity)

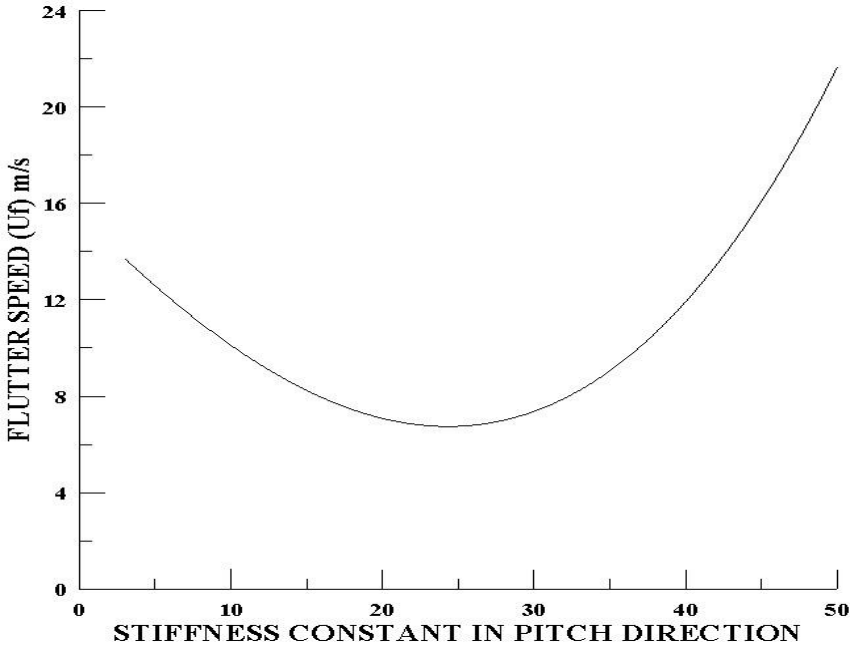

Figure -5.19 Variation between K_h and U_f

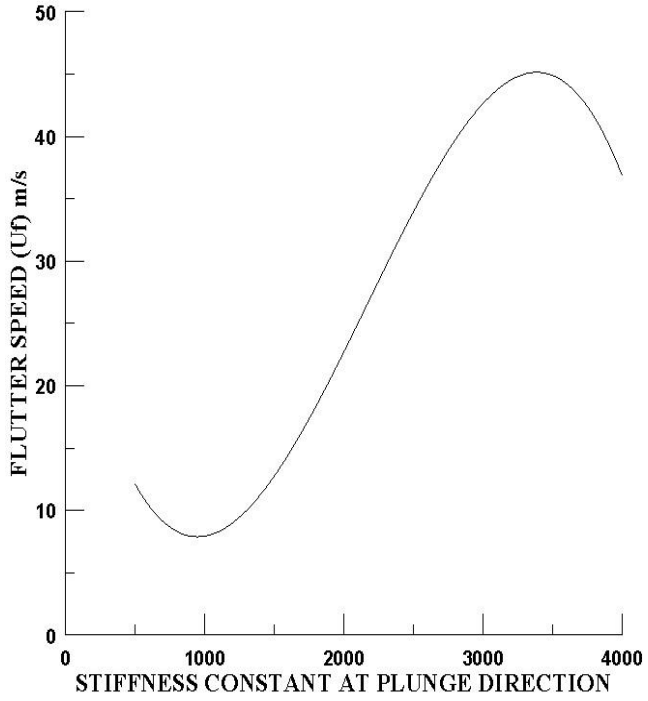

Figure-5.20 Variation between K_{α} and U_f

5.4 FINITE ELEMENT MODEL

The following data is used for the analysis:

(a) *Piezoelectric Material*

Length of piezo material =25 mm

Width =9.8 mm

Thickness =2 mm

Piezoelectric permittivity matrix

$$\varepsilon = \begin{bmatrix} 1800 & 0 & 0 \\ 0 & 1800 & 0 \\ 0 & 0 & 1800 \end{bmatrix}$$

Piezoelectric strain Matrix (m/V)

$$d = \begin{bmatrix} 0 & 0 & -1.9 \\ 0 & 0 & -1.9 \\ 0 & 0 & 3.9 \\ 0 & 0 & 0 \\ 0 & 5.84 & 0 \\ 5.84 & 0 & 0 \end{bmatrix} e-12$$

Anisotropic Elastic flexibility matrix $(N/m\hat{}2)^{-1}$

$$[c] = \begin{bmatrix} 1.52e-11 & -4.55e-12 & -5.77e-12 & 0 & 0 & 0 \\ 0 & 1.52e-11 & -5.77e-12 & 0 & 0 & 0 \\ 0 & 0 & 1.92e-11 & 0 & 0 & 0 \\ 0 & 0 & 0 & 5e-11 & 0 & 0 \\ 0 & 0 & 0 & 0 & 5e-11 & 0 \\ 0 & 0 & 0 & 0 & 0 & 3.94-11 \end{bmatrix}.$$

Density = 7800 kg/m^3

(b) *Shim Material (Isotropic Material)*

Elastic Modulus of shim= 66e9 N/m^2

Density of shim =8700 kg/m^3

Poissons Ratio = 0.3

Length of shim =25mm

Width =9.8mm

Thickness =1 mm

(c) Mass Material

Elastic Modulus of shim= 66e9 N/m^2

Density of shim =8700 kg/m^3

Poissons Ratio = 0.3

5.4.1 MODAL ANALYSIS

Modal analysis is used to find out the modes of vibration and corresponding natural frequencies.

The input providing to the modal analysis are:

Mode Extraction Method= Block Lanczos

Number of Modes to Extract= 10

Number of Modes to expand= 10

Frequency Range = 0-20000 Hz

The natural frequencies corresponding to vibrational modes are:

f_1=260.92 Hz f_2=826.58Hz

f_3=1785.2 Hz f_4=3696.7 Hz

f_5= 14380 Hz

5.4.2 HARMONIC ANALYSIS

Harmonic Analysis is used to determine the stedy state response of a linear structure to loads that varies sinusoidaly (harmonically) with time , thus enabling you to verify whether or not your design will successfully overcome resonance, fatigue and other harmful effect of forced vibrations. This analysis technique calculates only the steady state, forced vibration of a structure. The transient vibrations which occur at the beginning of vibration are not considered.

The following inputs are used for the Hamonic analysis are:

Solution Method- Full Load :1000N

Equation Solver: Sparse Solver Frequecy: 0-20000 Hz, Substeps:10

Variation of Displacements with Substeps Frequency of a Particular Node

The Fig21, Fig5.22 and Fig5.23 shows the variation of displacements in x,y and z direction respectively with respect to frequency. The above graphs are obtained from the ansys results. The graphs has drawn for a particular node displacement (say node no.50). The graphs show the harmonic vibration (displacement) of the particular node for a particular range of frequency steps.

1. Variation of U_x with Frequency

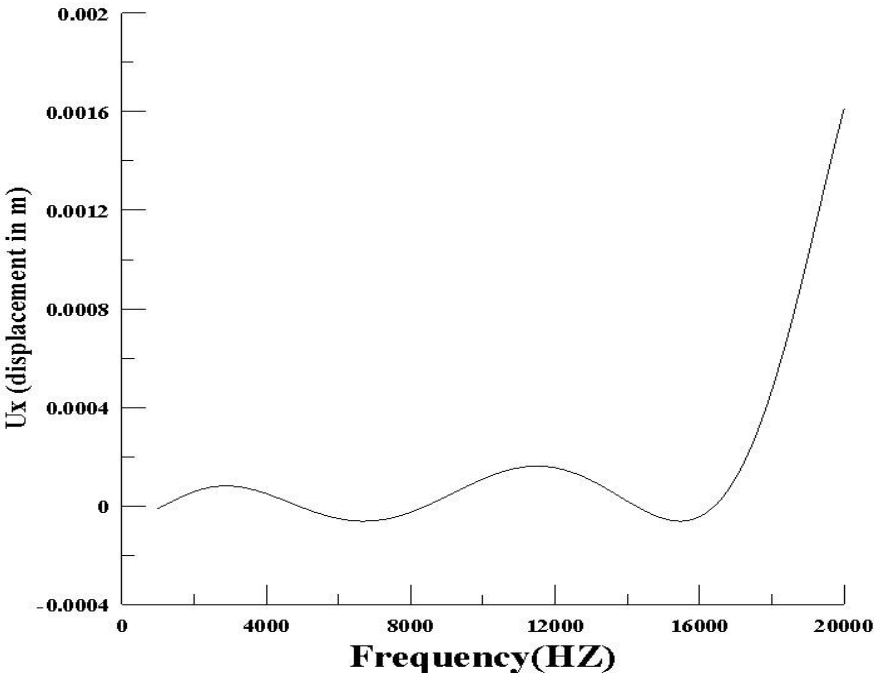

Fig5.21 Variation of U_x with Frequency

2. Variation of U_y with Frequency

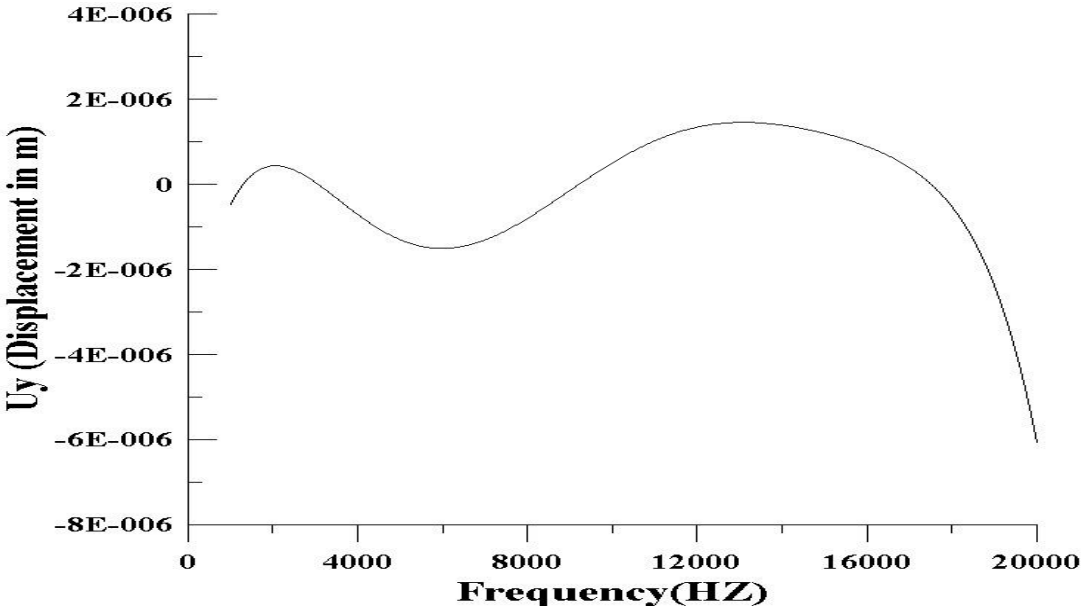

Fig5.22 Variation of U_y with Frequency

3. Variation of U_z with Frequency

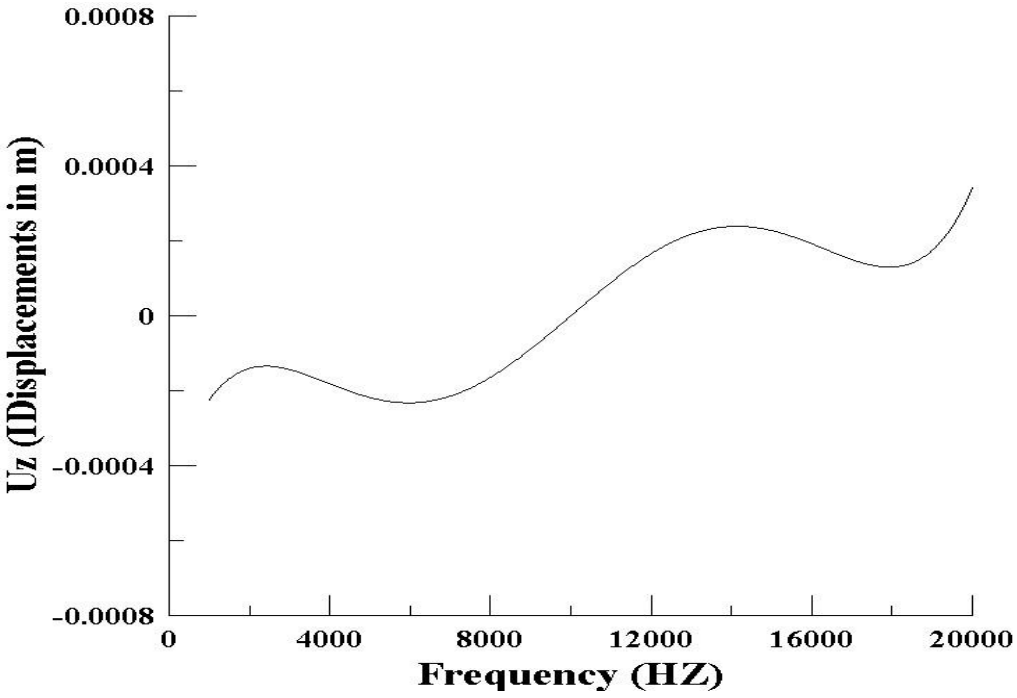

Fig5.23 Variation of U_z with Frequency

5.5 EXPERIMENTAL RESULTS

(a) Oscilloscope screen shot

The channel.1 shows the voltage variation with respect to time which is a output of piezoelectric element and channel.2 shows the variation of displacement with respect to time which is a output of accelerometer. The above graph shows the variation of magnitudes at 1000 Hz. The scaling factor is taking as 10 mV for voltage and 1 mV for displacement value.

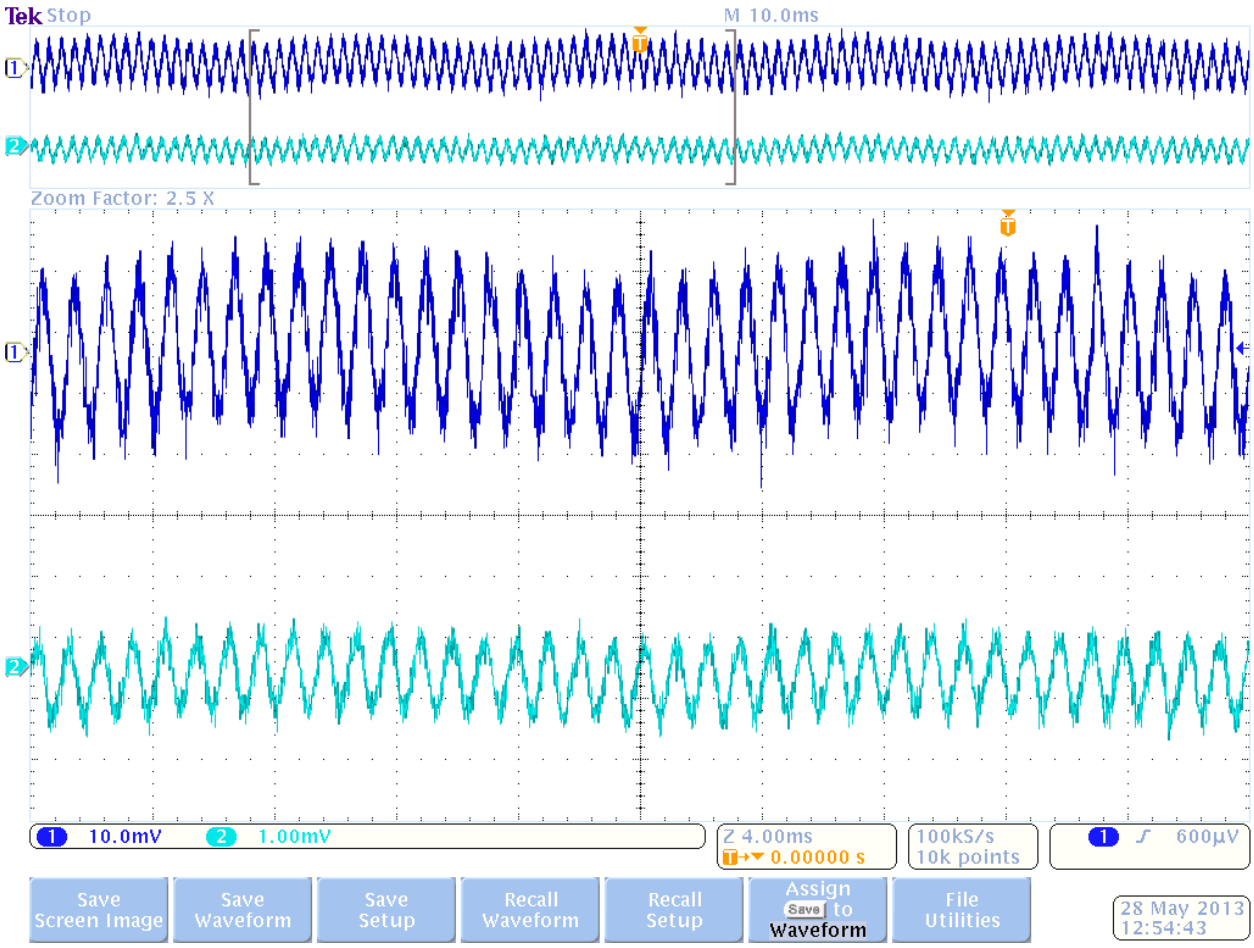

Fig5.24 Variation of voltage and Displacement with time in Osciloooscope

(b) Sine sweep result

From the sine sweep test the Fig 5.25 is derived. The graph shows the variation of voltage with respect to frequency. When the excitation frequency is matched with the natural frequency of beam i.e. at resonance condition the maximum amount of voltage is obtained. Here in the graph the maximum amount of voltage is obtained approximate 1000 Hz which is just close to the frequency obtained from the fundamental frequency formula of beam for first mode shape which is 827 Hz.

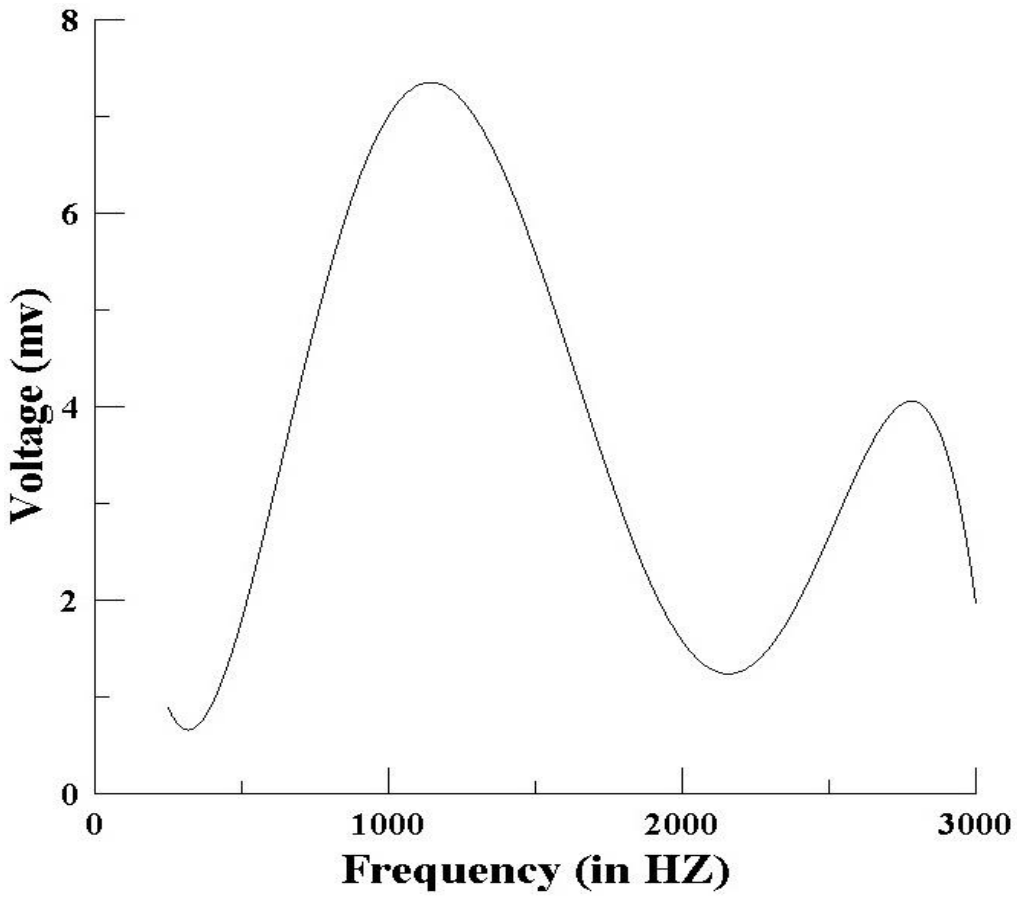

Fig5.25 Variation of voltage with Frequency

CHAPTER-6

CONCLUSIONS

This chapter describes the overall summary of the all models including the beneficial advantages of models and also describes the future scopes of all models.

6.1 SUMMARY

Modeling of piezoelectric bimorph cantilever beams has been conducted using (i) distributed parameter model (ii) lumped parameter model and (iii) finite element model. Solutions of distributed parameter model were obtained from assumed modes method where the first mode was employed for illustration sake. One and two degree of freedom lumped-parameter spring-mass models were used to idealize the bimorph cantilever structure. In a lumped parameter analysis using a single degree of freedom model, it is observed that the resonance occurs over a very narrow frequency bandwidth as for a linear system. So, it is very difficult to harvest maximum amount of power from this narrow operating region as the environment frequencies may not match always with the model frequency. In single degree of freedom we can harvest power only at resonance condition or very near to the resonance condition.

A two-degree of freedom wide band energy harvester design has been proposed to enhance the workability of conventional piezoelectric energy harvesters. For smaller peak distances, the mass ratio should be as low as possible, which facilitates also in decrease of total weight. The magnitudes of the first peak increases with mass ratio, while that of the second peak decreases. Even magnitudes are smaller than that of single DOF piezoelectric harvester, both the peaks have significant contribution to energy harvesting at lower mass ratios. The natural frequency is obtained from single degree and two degree of model as 720 Hz which is close to the frequency obtained from the distributed parameter model.

Just like, base excited cantilever harvesting system, it was shown the energy harvesting approach from aeroelastic systems like wings and cylinders. The amount of energy that can be harvested from a piezoaeroelastic system having a pitching and plunging rigid aerofoil supported by linear springs depends on its parameter and wind speed. The analysis shows the harvested power can be increased by choosing optimal parameters value. This analysis also shows that the harvested power increased at lowers flutter speeds.

Finite element analysis is performed using multiphysics options of ANSYS software. The results show that second natural frequency obtained is approximately equal to the natural frequency obtained from the mathematical formula of finding the natural frequency of the cantilever beam. The validation of result is also followed by an experiment. A one inch brass cantilever with two piezo patches and a tip mass was used to extract the vibrations from base. The sine sweep test validates the result and shows that the maximum amount of voltage (7.5mV) is generated at approximately 1000Hz.

6.2 FUTURE SCOPE

As we see from the above discussion the distributed parameter model is solved only with Euler-Bernoulli approach. The further work of distributed parameter model will be carried out by adopting Timoshenko model and Rayleigh beam models. Single degree of freedom lumped parameter model studied in present work should be added with nonlinear terms to enhance the bandwidth slightly. From the piezoaeroelastic model, the further work would be carried out by adopting the nonlinear terms in lift and pitching moments and then can be gone for optimizing the parameters to harvest maximum power. Further, the experiment shows a very less amount of voltage generated, so the future work is to improve the device and use of piezoelectric element with high piezoelectric constants to get maximum amount of voltage.

REFERENCES

1. P.Mitcheson, P.Miao, B.Start, E.Yeatman, A.Holmes and T.Green, 'MEMS electrostatic micro-power generator for low frequency operation', Sensors and Actuators A, Phys., Vol.115, pp.523–529, 2004.
2. S.R.Anton and H.A.Sodano, 'A review of power harvesting using piezoelectric materials (2003–2006)', Smart Materials and Structures, Vol.16, pp.1–21, 2007.
3. K.A.Cook-Chennault, N.Thambi, and A.M.Sastry, 'Powering MEMS portable devices-a review of non-regenerative and regenerative power supply systems with emphasis on piezoelectric energy harvesting systems', Smart Mater. Struct. Vol.17, p.043001, 2008.
4. S.P.Beeby, M.J.Tudor and N.M.White, 'Energy harvesting vibration sources for microsystems applications', Meas. Sci. Technol., vol.17, pp.175–195, 2006.
5. H.A.Sodano, D.J.Inman, and G.Park, 'A review of power harvesting from vibration using piezoelectric materials', Shock Vib. Dig., vol. 36, pp.197–205, 2004.
6. S.Priya, 'Advances in energy harvesting using low profile piezoelectric transducers', J. Electroceram., vol.19, pp.167–184, 2007.
7. H.Sodano, G.Park and D.J.Inman, 'Estimation of electric charge output for piezoelectric energy harvesting', Strain, vol. 40, pp.49–58, 2004.
8. A.Erturk and D.J.Inman, 'An experimentally validated bimorph cantilever model for piezoelectric energy harvesting from base excitations', Smart Materials and Structures, vol.18, 025009, 2009.
9. A.Erturk and D.J.Inman, 'On mechanical modeling of cantilevered piezoelectric vibration energy harvesters', J. Intell. Mater. Syst. Struct., vol.19, pp.1311–1325, 2008.

10. A.Erturk and D.J.Inman, ‘A distributed parameter electromechanical model for cantilevered piezoelectric energy harvesters’, J. Vib. Acoust., vol.130, 041002, 2008.
11. M.Umeda, K.Nakamura, and S.Ueha, S, ‘Analysis of transformation of mechanical impact energy to electrical energy using a piezoelectric vibrator’, Japanese Journal of Applied Physics, vol. 35, pp.3267–3273, 1996.
12. M.Goldfarb and L.D.Jones, ‘On the efficiency of electric power generation with piezoelectric ceramic’, ASME Journal of Dynamic Systems, Measurement, and Control, vol.121, pp.566–571, 1999.
13. N.G.Elvin, A.A.Elvin and M.Spector, ‘A self powered mechanical strain energy sensor’, Smart Materials and Structures, vol.10, pp.293–299, 2001.
14. H.A.Sodano, E.A.Magliula, G.Park and D.J.Inman, ‘Electric power generation from piezoelectric materials’, In: The 13th International Conference on Adaptive Structures and Technologies, 7–9 October, 2002, Potsdam, Berlin, Germany.
15. W.J.Wu, Y.Y.Chen, B.S.Lee, J.J.He and Y.T.Pen, ‘Tunable Resonant Frequency Power Harvesting Devices’, Proc. SPIE, 6169, pp. 81–92, 2006.
16. O.Aldraihem and A.Baz, ‘Energy harvester with a dynamic magnifier’, Journal of Intelligent Material Systems and Structures 22: 521–530, 2011.
17. H.Y.Wang, X.B.Shan and T.Xie, ‘An energy harvester combining a piezoelectric cantilever and a single degree of freedom elastic system’, J.Zhejiang University-Sci A, (Applied Physics & Eng), vol.13, pp.526-537, 2012.
18. J.E.Kim and Y.Y.Kim, ‘Analysis of piezoelectric energy harvesters of a moderate aspect ratio with a distributed tip mass’, J. Vibration and Acoustics, Trans.ASME, vol. 133, pp,0410101-16, 2011.

19. L.Zhou, J.Sun, X.J.Zheng, S.F.Deng, J.H.Zhao, S.T.Peng, Y.Zhang, X.Y.Wang and H.B.Cheng, 'A model for energy harvesting performance of shear mode piezoelectric cantilever', Sensors and Actuators, A, vol.179, pp.185-192, 2012.
20. K.H.Mak, S.McWilliam, A.A.Popov and C.H.J.Fox, 'Peformance of a cantilever piezoelectric energy harvester impacting a bump stop', J.Sound and Vibration, vol.330, pp.6184-6202, 2011.
21. A.Erturk, 'Assumed-modes modeling of piezoelectric energy harvesters: Euler-Bernoulli, Rayleigh and Timoshenko models with axial deformations', Computers and Structures, vol.106-107, pp.214-227, 2012.
22. S.Zhao and A.Erturk, 'Electroelastic modeling and experimental validations of piezoelectric energy harvesting from broadband random vibrations of cantilevered bimorphs', Smart Materials and Structures, vol. 22, pp.015002, 2013.
23. L.Tang and Y.Yang, 'A multiple-degree of freedom piezoelectric energy harvesting model', J.Intelligent Material Systems and Strctures, vol.24, pp.357-368, 2012.
24. M.F.Lumentut and I.M.Howard, 'Analytical and experimental comparisons of electromechanical vibration response of a piezoelectric bimorph beam for power harvesting', Mechanical Systems and Signal processing, vol.36, pp.66-86, 2013.
25. H.Wang and Q.Meng, 'Analytical modeling and experimental verification of vibration based piezoelectric bimorph beam with an tip-mass for power harvesting', Mechanical Systems and Signal processing, vol.36, pp.193-209, 2013.
26. I.L.Cassidy and J.T.Scruggs, 'Nonlinear stochastic controllers for power-flow constrained vibratory energy harvesters', J.Sound and Vibration, vol.332, pp.3134-3147, 2013.

27. M.Bryant and E.Garcia, ‘Development of an aeroelastic vibration power harvester’, Proc. SPIE 7288, 728812, doi:10117/12.815785, 2009.
28. A.Erturk, W.G.R.Vieira, C.De Marqui and D.J.Inman, ‘On the energy harvesting potential of piezoaeroelastic systems’, Appl. Phys. Lett., vol. 96, p.184103, 2010.
29. C.De Marqui, A.Erturk, and D.J.Inman, ‘Piezoaeroelastic modeling and analysis of a generator wing with continuous and segmented electrodes’, J. Intell. Mater. Syst. Struct., vol.21, pp.983–993, 2010.
30. A.Abdelkefi and A.H.Nayfeh and M.R.Hajj, ‘Modeling and analysis of piezoaeroelastic energy harvesters’, Nonlinear Dynamics, vol.67, pp.925-939, 2012.
31. A.Abdelkefi, A.H.Nayfeh and M.R.Hajj, ‘Design of piezoaeroelastic energy harvesters’, Nonlinear Dynamics, vol.68, pp.519-530, 2012.
32. C.De Marqui and A.Erturk, ‘Electroaeroelastic analysis of airfoil-based wind energy harvesting using piezoelectric transduction and electromagnetic induction’, J.Intelligent Material Systems and Strctures, DOI: 10.1177/1045389X12461073

APPENDIX-1

ANSYS APDL COMMAND TO GENERATE SOLID MODEL AND MESH

```
/clear
/COM,Bimorph Model
/FILNAME, Bimorph,0
/TITLE, Bimorph Power Analysis
*SET,Lm,5E-3 !Length of mass
*SET,Hm,9.8E-3 !Height of mass
*SET,Wb,9.8E-3 !Width of mass
*SET,Lb,25E-3 !Length of beam
*SET,Lp,20E-3! Length of pizo
*SET,Tp,0.14E-3 !Pizeoelectric Thickness
*SET,Tsh,0.26E-3 !Shim Thickness
/UNITS,MKS ! MKS system (m, kg, s, °C#
/PREP7
local,11
local,12,,,,,,180,,
ET,1,SOLID45  !Set Element Types
ET,2,SOLID5,3
ET,3,CIRCU94,0
CSYS,11
BLOCK,0,Lb,0,Wb,0,Tsh,  !Draw Shim
BLOCK,0,Lp,0,Wb,Tsh,Tsh+Tp, !Drawing Top Pizeoelectric Layer
BLOCK,0,Lp,0,Wb,0,-Tp,  !Drawing Bottom Pizeoelectric Layer
BLOCK,Lp,Lp+Lm,0,Wb,Tsh,Tsh+Hm,
EMUNIT,    MKS,  ! Define Piezoelectric  Material Model
MPTEMP, 1, 25, , , , , ! PZT Density
MPDATA,DENS,1,,7800
TB,PIEZ,1,,,0   ! Piezoelectric matrix
TBDATA,    3,    -12
TBDATA,    6,    -12
TBDATA,    9,    18.2
TBDATA,    14,    21.9
TBDATA,    16,    21.9
MPTEMP, 1, 25, , , , , ! Clamped Dielectric Constant
MPDATA,PERX,1,,1800
MPDATA,PERY,1,,1800
MPDATA,PERZ,1,,1800
TB,    ANEL,    1,1,0 ! Anisotropic elastic matrix
TBTEMP,25
MPTEMP, 1, 25, , , , , ! Define Shim #Brass) Material Model
MPDATA,DENS,2,,2700 ! Density of Shim
MPDATA,EX,2,,69E9  ! Elastic Modulus of  Shim
MPDATA,PRXY,2,,0.3 ! Poissons Ratio of Shim
MPTEMP, 1, 25, , , , , ! Define Mass #Tungsten Alloy) Material Model
MPDATA,DENS,3,,8470 ! Density of Mass
MPDATA,EX,3,,1E11 ! Elastic Modulus of  Mass
MPDATA,PRXY,3,,0.3  ! Poissons Ratio of Mass
VSEL,All
VGLUE,ALL    ! Combine all Volumes
VSEL,S,LOC,Z,0,Tsh, , ! Defining Element Type & Material Properties of layers
VSEL,R,LOC,X,0,Lb, ,
NSEL,R,LOC,Y,0,Wb, ,
VATT,      2, ,   1,      11  !Shim Layer
VSEL,S,LOC,Z,Tsh,Tsh+Tp, ,
VSEL,R,LOC,X,0,Lp, ,
NSEL,R,LOC,Y,0,Wb, ,
VATT,    1, ,   2,      11  !Top Pizeoelectric Layer
VSEL,S,LOC,Z,0,-Tp, ,
```

```
VSEL,R,LOC,X,0,Lp, ,
NSEL,R,LOC,Y,0,Wb, ,
VATT,     1, ,   2,      11 !Bottom Pizeoelectric Layer
VSEL,S,LOC,Z,Tsh,Tsh+Hm, ,
VSEL,R,LOC,X,Lp,Lp+Lm, ,
NSEL,R,LOC,Y,0,Wb, ,
VATT,      3, ,  1,       11 ! Mass
ESIZE,4E-4,0, ! Mesh Size
VSEL,ALL
VSWEEP,All !Sweep Volumes
ASEL,S,LOC,X,0,,,  ! Fixing End of Shim
 DA,ALL,UX,0,,
 DA,ALL,UY,0,,
DA,ALL,UZ,0,,
ALLSEL,ALL
/REPLOT
FINISH
```

APPENDIX-2

Runga Kutta Solver General Steps

The fourth order R.K. Solver method can be summarized by the following equations,

$K1= f(x_n , y_n)h$

$K2= f (x_n+ 0.5h, y_n+0.5K1)*h$

$K3= f(x_n+ 0.5h, y_n+0.5K2)*h$

$K4= f(x_n+h , y_n+K3)*h$

$Y_{n+1}= y_n+ (1/6)(K1+2*K2+2*k3+K4) +O(h^5)$

APPENDIX-3

MODE SHAPE FOR THE CANTILEVER BEAM

Mode shape for the cantilever beam,

$$\varphi(x) = A\cos\beta x + B\sin\beta x + C\cosh\beta x + D\sinh\beta x \quad \text{(A.1)}$$

Boundary Conditions,

1. At x=0, $\phi_r(x)=0$

2. At x=0, $\phi'_r(x)=0$ (slope)

3. At x=l, $EI\phi''_r(x)=0$ (Moment)

4. At x=l, $EI\,\phi'''_r = M_t\ddot{w}$ (Shear Force)

As we assume that the displacement of the beam,

$y = \phi(x)w(t)$

$w(t)$ - Non- dimensional co-ordinate

After putting the boundary condition,

A+C=0 (A.2)

B+D=0 (A.3)

From third boundary condition ,

$$A[\cos(\beta l) + \cosh(\beta l)] + B[\sin(\beta l) + \sinh(\beta l)] = 0 \quad \text{(A.4)}$$

From fourth boundary condition,

And put also $w(t) = w_0 e^{j\omega t}$

$\ddot{w}(t) = -w_0 \omega^2 e^{j\omega t}$

$$A[(\sinh(\beta l) - \sin(\beta l)) + \alpha_0(\beta l)(\cosh(\beta l) - \cos(\beta l))]$$

$$+ B[(\cos(\beta l) + \cosh(\beta l)) - \alpha_0(\beta l)(\sin(\beta l) - \sinh(\beta l))] = 0 \qquad \text{(A.5)}$$

To find the frequency equation, the determinant of equation (A.4) and (A.5) equals to zero,

$$\begin{vmatrix} (\sinh(\beta l) - \sin(\beta l)) + \alpha_0(\beta l)(\cosh(\beta l) - \cos(\beta l)) & (\cos(\beta l) + \cosh(\beta l)) - \alpha_0(\beta l)(\sin(\beta l) - \sinh(\beta l)) \\ \cos(\beta l) + \cosh(\beta l) & \sin(\beta l) + \sinh(\beta l) \end{vmatrix} = 0$$

The frequency equation-

$$1 + \cos(\beta l)\cosh(\beta l) + \alpha_0(\beta l)[\cos(\beta l)sinh(\beta l) - sin(\beta l)sinh(\beta l)] = 0 \qquad \text{(A.6)}$$

Where

α_0= Tip mass ratio $= \dfrac{M_t}{\rho A l}$

From equation(A.1)

$$\varphi(x) = A cos\beta x + B sin\beta x + C cosh\beta x + D sinh\beta x$$

Normalized mode shape function is given by,

$$\phi_b(x) = A[(\cos(\beta x) - \cosh(\beta x)) + C_1(\sin(\beta x) - \sinh(\beta x))]$$

$$C_1 = \frac{(\sinh(\beta l) - \sin(\beta l)) + \alpha_0(\beta l)(\cosh(\beta l) - \cos(\beta l))}{(\cos(\beta l) + \cosh(\beta l)) - \alpha_0(\beta l)(\sin(\beta l) - \sinh(\beta l))} \qquad (2.7)$$

Where A is normalized Mode Shape.